

Kinetic and gas-phase study of the chemical vapor deposition of silicon carbide from $C_2H_3SiCl_3/H_2$

A. Desenfant¹, G. Laduye², G. L. Vignoles¹, G. Chollon^{1*}

¹ Laboratoire des Composites Thermostructuraux, CNRS, Safran, CEA, University of Bordeaux, 3, Allée La Boétie, 33600 Pessac, France

² Innovation Campus Paris, Air Liquide, 781350 Les Loges en Josas, France

* Corresponding author [μ chollon@lcts.u-bordeaux.fr](mailto:chollon@lcts.u-bordeaux.fr)

Keywords: Chemical vapor deposition; Vinyltrichlorosilane; Silicon carbide; Deposition kinetics; FTIR Spectroscopy; Gas phase analysis

Abstract: The chemical vapor deposition (CVD) of silicon carbide from vinyltrichlorosilane (VTS) was studied to identify a range of conditions leading to pure crystalline SiC. The deposition rate was recorded to evidence the various deposition regimes. Gas phase, elemental analyses and infiltration tests were also performed. Three distinct chemical reaction regimes were identified. In CVD conditions, carbon is co-deposited at low temperature while VTS is only partially decomposed. In infiltration conditions, the composition switches to pure SiC inside the porous substrate because of a depletion of reactive hydrocarbon species. Competing heterogeneous reactions are responsible for a hysteresis versus temperature, in both deposition rate and composition of the deposit. The high temperature domain is the most suitable to deposit pure crystalline SiC in CVD conditions. Hydrogen dilution strongly accelerates the homogeneous decomposition of VTS as compared to argon. Assumptions on the reaction mechanism were proposed describing the chemistry of this precursor.

1. Introduction

SiC/SiC composites are of great interest for use in aircraft engines and nuclear reactors. Their low density and high strength at high temperature make them good candidates to replace metallic alloys for such applications [1,2]. Chemical vapor infiltration (CVI) is often used to manufacture the

silicon carbide matrix, since it enables the deposition of pure SiC inside the fibrous substrate [3]. The most used precursor for the chemical vapor infiltration (CVI) of SiC is methyltrichlorosilane (MTS, CH_3SiCl_3) diluted in hydrogen. This process often leads to some silicon excess at low temperature and low gas residence time [4,5], leading to a decrease of the lifetime of the final material [6]. Previous works from the literature mentioned that both the high reactivity of chlorosilanes and the low reactivity of hydrocarbons formed in the gas phase at low temperature could explain the low carbon content in the deposit [4,7–10]. Some authors have proposed to add HCl in order to promote silicon etching [17,11–13]. Others suggested to supply additional hydrocarbons, such as CH_4 [14], C_3H_8 [15], C_2H_2 [16] or C_2H_4 [17] in the MTS/ H_2 mixtures, to counterbalance the silicon excess and enable pure SiC deposition. Another solution could be to use a single-source precursor with a higher carbon content, for instance $\text{C}_2\text{H}_5\text{SiCl}_3$ [18–21], $(\text{CH}_3)_2\text{SiCl}_2$ [22–28], $(\text{CH}_3)_3\text{SiCl}$ or $(\text{CH}_3)_4\text{Si}$ [27], to form pure SiC. The latter solution was chosen in the present work, by studying the feasibility of using an original molecule, vinyltrichlorosilane (VTS), $\text{C}_2\text{H}_3\text{SiCl}_3$, as a precursor of pure SiC deposit in both CVD and CVI conditions. Unsaturated hydrocarbons are indeed likely to form from the vinyl group in the early stages of the VTS decomposition. The high heterogeneous reactivity of these species should favor carbon deposition and thus the formation of pure SiC.

The second important aspect of this work is to improve the SiC infiltration capacity into porous substrates. Regarding the MTS/ H_2 system, Papasouliotis *et al.* noticed that the deposition rate and SiC mole fraction strongly depend on the distance of the substrate from the beginning of the hot zone, probably due to an increasing HCl content []. As a result, they estimated that it is necessary to increase the residence time to achieve uniform infiltration of SiC in a porous preform with this precursor. Zhang and Hüttinger have observed the same phenomenon with the deposition rate and Si co-deposition depending on the position of the substrate in the reactor [5]. They also studied the influence of the substrate surface area/reactor volume (A_s/V_r) ratio, by using three different substrates, and noticed that more free Si was co-deposited when A_s/V_r was decreased. According to these authors, this effect could be due to the formation of heavier chlorosilane and carbochlorosilane species at low A_s/V_r ratio [5,2]. It could be responsible for a non-homogeneous composition of the solid deposited by CVI in porous substrates.

The aim of the present study is to consider VTS as a potential precursor for the CVI of pure and crystalline SiC coatings with a high thickness uniformity. The influence of the CVD parameters

has been examined through a kinetic study of the deposition rate, chemical and structural analysis of the solid deposit and infrared spectroscopy investigations of the gas-phase. Correlations between the various experimental results and data from the literature allowed proposing a basic homogeneous / heterogeneous reaction mechanism for the CVD of SiC from VTS. Finally, the CVI capability of this precursor has been studied through model pore infiltration [30].

2. Experimental procedure

Vinyltrichlorosilane (Sigma Aldrich, 97 %) is liquid at ambient pressure and temperature (boiling temperature: 90 °C). It was injected in a vertical hot-wall CVD reactor (presented in Fig. 1) by a bubbling system with a dew point column in order to regulate the flow rate. The diluent gases (H₂ or Ar, . . . %, from Air Liquide) and the precursor flowed through a vertical silica tube (700 mm long and 34 mm inside diameter) heated by a graphite susceptor (130 mm long and 55 mm inside diameter) coupled to a radio-frequency inductive coil.

The reactor pressure P was fixed using a motorized valve and a Baratron® pressure gauge (both from MKS). The temperature in the reactor was monitored by a K type thermocouple inserted in the susceptor wall. The deposition temperature T of the substrate and the isothermal hot-zone (50 mm long, at ± 5 °C) were determined by recording thermal profiles prior to the CVD and CVI experiments with another thermocouple moving along the reactor axis (examples temperature profiles are given in reference [30]).

The reactor was connected to a high-sensitivity microbalance (B Setsys from Setaram, sensitivity ± 1 ng) to which the specimen was hung allowing the *in situ* acquisition of the weight gain. The substrates used consisted in dense graphite (2318 PT from Mersen) cylindrical pins, 1 cm in height and diameter, with an outer surface of 4.71 cm². The deposition rate R , in mg.min⁻¹.cm⁻², was calculated by dividing the weight gain by the geometrical substrate surface. The open pores of the substrates were filled by a few microns-thick SiC coating to get a constant surface area before each run for reproducible measurements of R . Repeatability tests were carried out for every CVD condition tested. Several layers of CVD-SiC coating were deposited on the same substrate during the same run, by cutting off the reactant gas supply between each condition and modifying the temperature (500 – 1150 °C), pressure (2 – 10 kPa), the set point for the VTS ($Q_{VTS} = 5 - 30$ standard cubic centimeters per minute, or sccm) or diluent gas flow rate (either hydrogen or argon,

$Q_{H_2/Ar} = 100 - 500$ sccm), and by letting the reactant gases flow again. The state of equilibrium of the temperature, pressure and H_2 flow was carefully monitored *in situ* with the microbalance before introducing the reactant gases (the microbalance is extremely sensitive to any variation of T , P or gas flow).

A Fourier transform infrared (FTIR) spectrometer (IS50 from ThermoScientific) was also coupled to the CVD reactor at the outlet for *ex situ* gas-phase analysis. 32 scans with a 0.5 cm^{-1} resolution were recorded for each spectrum. The background was recorded prior to the gas analysis for each temperature condition but under a pure H_2 flow to calculate the absorbance spectra. Repeatability tests were also carried out for every condition to confirm the occurrence of a steady-state regime. Quantitative concentration measurements were carried out by calibration using pure gases, when available, at various partial pressures.

The microstructure of the deposited films was examined using a scanning electron microscope (SEM, Quanta-400 FEG from FEI) equipped with an energy-dispersive X-ray spectroscopy (EDS) analysis module.

The structural organization of the SiC phase and the presence of secondary phases (free silicon or free carbon) was assessed by Raman microspectroscopy (Labram HR from Horiba Jobin-Yvon) ($\lambda = 632.8\text{ nm}$, spectral resolution 2 cm^{-1} , lateral resolution $1\text{ }\mu\text{m}$) and X-ray diffraction (XRD, D5000 from Siemens, $\lambda_{Cu-K} = 0.1542\text{ nm}$, functioning in the -2θ configuration).

The elemental composition of the coatings was controlled by electron probe micro-analysis (EPMA, SX 100 from CAMECA, source: 15 kV, 20 nA). The Si and O weight concentrations were quantified with respectively LPET and PC1 crystals and the C concentration calculated by difference (SiC and SiO_2 were used as standards).

3. Results

3.1. Influence of the temperature

In a first experiment, the deposition temperature T was varied from 600 to 1150 °C, the total pressure P was set at 2 kPa, the total flow-rate Q_{tot} at 150 sccm and the dilution ratio $a = Q_{H_2}/Q_{VTS}$ at 13. The Arrhenius plot of the deposition rate R is given in Fig. 2a. The partial pressures of the various gas species detected in parallel by FTIR at the outlet of the reactor are presented versus

temperature in Fig. 2b. The deposition rate remains low ($< 2.10^{-3} \text{ mg}\cdot\text{min}^{-1}\cdot\text{cm}^{-2}$) when increasing temperature from 25 to 75 °C. R increases with T with an apparent activation energy of approximately 250 $\text{kJ}\cdot\text{mol}^{-1}$. The EDS and Raman analyses (Fig. 3a) performed on a coating deposited at 50 °C in steady-state conditions showed that the deposit consists mainly of carbon and only small amounts of silicon (5 at. %) and chlorine (0.8 at. %). High resolution TEM analyses only reveal short and distorted carbon 002 lattice fringes, with some degree of anisotropy, similarly as in a highly disordered pyrolytic carbon (Fig. 3b) [31]. Traces of oxygen were also detected (2 at. %), which may be due to oxygen or moisture adsorption during exposure to ambient air after deposition, possibly in relation with the presence of residual chlorine. The FTIR measurements at the reactor outlet show that VTS is scarcely decomposed at these temperatures, to form SiHCl_3 , C_2H_4 and a small amount of C_2H_2 . Traces of SiH_2Cl_2 were also detected but could not be quantified (the pure species could not be analyzed so the molar absorption coefficient could not be determined).

A further increase of temperature from 75 to 1000 °C leads to an abrupt rise of R of more than one order of magnitude. Within this temperature domain, the deposit composition suddenly turns from nearly pure carbon to pure SiC (Figs. 4 and 5), indicating an important change in the heterogeneous reaction scheme. Simultaneously, a maximum of the SiHCl_3 concentration is observed at the reactor outlet approaching 1000 °C, while the ethylene concentration strongly increases.

Between 1000 and 1100 °C, the deposition rate remains high and the apparent activation energy, of the order of 200 $\text{kJ}\cdot\text{mol}^{-1}$, slightly decreases with increasing temperature. The solid deposited consists of pure polycrystalline β -SiC (Figs. 4 and 5), with a crystallinity gradually improving with T (Fig. 4). The coating obtained at $T = 1100$ °C displays columnar grains having 111 axes oriented mainly along the growth direction and containing stacking faults (Fig. 6). The outlet ethylene and SiCl_4 concentrations reach a maximum, while the SiHCl_3 content exhibits a constant decrease. The very low VTS concentration detected downstream of the hot zone reveals that the precursor is almost totally decomposed.

For temperatures above 1100 °C, the apparent activation energy becomes very low (it can be estimated below 50 $\text{kJ}\cdot\text{mol}^{-1}$). Between 1100 and 1150 °C, the elemental and Raman analyses show that free carbon is incorporated in the deposit in proportions increasing with temperature (Fig. 4).

In the gas phase at the reactor outlet, the increase of temperature above 1100 °C results in a decrease of the concentrations of C₂H₄ and SiCl₄, while the concentration of acetylene increases.

During the decrease of the temperature from 1150 °C back to 50 °C, the deposition rate follows the same Arrhenius law as observed during temperature increase. No hysteresis of R with temperature was evidenced in these conditions.

The gas, solid and total mass yields of the carbon, silicon and chlorine elements were calculated respectively from the FTIR analyses at the reactor outlet, the temperature dependence of both the deposition rate and the composition of the deposit on the substrate and reactor walls (at $P = 2$ kPa, $\phi = 13$ and $Q_{\text{tot}} = 150$ sccm, see Fig. 7). The contribution of SiH₂Cl₂ was not considered since this species was not quantified (see above). To simplify, the influence of the residence time on R along the temperature profile outside of the hot zone was also neglected (R was supposed to depend only on T on both sides of the hot zone). This assumption is valid in case of a surface reaction limitation (or chemical reaction regime, CRR) but not in a mass transfer regime (MTR). The deposition downstream on the cooler parts of the reactor was not considered. As expected, when T increases, the amounts of Si and C in the gas phase both decrease while those in the solid both increase (Fig. 7a,b). An elemental deficit in the total mass yield appears from 25 °C and reaches a maximum at 1050 °C for Si and C and 1100 °C for Cl (Fig. 7c). Such a discrepancy in the mass yields could be related to the failure to consider some gaseous species (*e.g.* SiH₂Cl₂). It can be more likely attributed to the deposition of heavy species on the cold parts of the reactor [5]. Indeed, after several experiments, the replacement of the reactor tube revealed the presence of a brown solid, possibly similar to that collected by Cagliostro *et al.* during their CVD study from (CH₃)₂SiCl₂/Ar mixtures [23]. The FTIR analysis evidenced that this compound originally contained Si-Cl and Si-H bonds that readily reacted with ambient air to form Si-O-Si bonds. The resulting white powder was found by EDS to be composed of about 40 at. % of C, 25 at. % of Si and 33 at. % of oxygen (a strong luminescence prevented any phase analysis by Raman spectroscopy). The solid Si and C mass yields reach up to 0 % and 46 % respectively at 1050 °C ($P = 2$ kPa, $\phi = 13$ and $Q_{\text{tot}} = 150$ sccm, Fig. 7a,b). This result indicates that the high depletion of the precursors at the reactor outlet and probably also in the hot zone is a direct consequence of heterogeneous reactions occurring at high temperatures.

3.2. Influence of the total pressure

In addition to the previous run at 2 kPa, two additional experiments were conducted to follow the thermal behavior of the deposition rate and the gas phase at 5 and 10 kPa (Figs. 8 and). The total flow rate and the dilution ratio were both kept constant to assess the influence of the total pressure on the deposition of SiC from VTS-H₂. The increase of the initial partial pressure of VTS (resulting from the rise of the total pressure) leads to a shift of the Arrhenius plot towards lower temperatures (for clarity, the three Arrhenius curves are compared on the same plot in Fig. SI1 in the Supplementary Information). Except this temperature shift, the overall curve shape, the apparent activation energies of the different regimes and the evolution of both the gas phase and the composition of the deposit are similar at 5 kPa to those observed at 2 kPa (Figs. 2,5,8,SI1). A similar behavior was observed for the CVD of SiC from MTS/H₂ mixtures [32].

In contrast with the 2 kPa experiment, a hysteresis phenomenon was observed in the Arrhenius plots of the deposition rate at 5 and 10 kPa. In the low-temperature part of the curve, the R value at a given temperature was found lower (respectively higher) when the deposition temperature was increasing (respectively decreasing), as shown in Figs 8a and a. A hysteresis phenomenon was also observed in the change of the deposit composition. Pure silicon carbide was formed along the high deposition rate branch of the Arrhenius plot (*i.e.* upon cooling), whereas a carbon-rich coating was deposited along the low R branch (on heating). The hysteresis was also observed at 2 kPa, but for a dilution ratio α of 20 instead of 13 (see Fig. SI2 in Supplementary Information). On the other hand, for the various pressures and dilution ratios, no significant change was observed in the composition of the gas phase for the two hysteresis branches in the Arrhenius plots.

At 10 kPa, the kinetic behavior is significantly different from that observed at 2 and 5 kPa. An intermediate linear domain appears in the Arrhenius plot in the range $T = 800 - 1000$ °C (Fig. a), between the low temperature (with hysteresis) and high temperature domains. The related apparent activation energy is significantly higher ($250 \text{ kJ}\cdot\text{mol}^{-1}$) than that measured in the high temperature domain of the Arrhenius plots at 2 kPa ($T > 1000$ °C), 5 kPa ($T > 800$ °C) and 10 kPa ($T > 1000$ °C). This specific kinetic regime suggests that conditions combining high pressures and intermediate temperatures may induce some changes in the reaction mechanism or at least in the limiting step of the deposition process. In this intermediate T domain, the C₂H₄ and SiCl₄ outlet concentrations both increase with T , while the SiHCl₃ concentration starts to decrease (Fig. b)

and the solid deposited consists of pure SiC (Fig. 5). The C₂H₄ and SiCl₄ concentrations then decrease when T further increases, in the high temperature domain ($1000 < T < 1125$ °C). The C₂H₂ concentration significantly increases in parallel, while a large carbon excess appears in the solid.

3.3. Influence of the total flow rate

At a pressure of 2 kPa, the increase of the total flow rate (Q_{tot}) leads to different behaviors of the deposition rate depending on the temperature (Fig. 10). For $T = 1075$ °C or $T = 1100$ °C, R strongly increases with Q_{tot} over the entire range tested. This behavior is characteristic of a mass transfer limitation, as already suggested by the very low thermal activation on the Arrhenius plot (Fig. 2a, see section 3.1). The deposition rate tends to be less influenced by the total flow rate at 1025 °C, indicating a mixed limitation by both surface reactions and diffusion.

Fig. 11a displays the change in the gas phase composition at the reactor outlet as a function of the residence time τ_R (as calculated from the total flow rate Q_{tot}) at $P = 2$ kPa, $\alpha = 13$, and $T = 50$ °C. Although the effect is less pronounced, a parallel can be drawn with the gas phase changes observed when increasing the temperature of the hot zone (Fig. 2b). VTS gets slightly more decomposed as τ_R increases (or Q_{tot} decreases), resulting in slightly more products at the reactor outlet.

The effect of τ_R on VTS decomposition is still effective at 1100 °C, while VTS is much more decomposed and the gas products much more abundant than at 50 °C (Fig. 11b). On the other hand, the partial pressures of SiHCl₃ and C₂H₄ now decrease when τ_R increases, also as expected from the parallel with the temperature effect shown in Fig. 2b. The influence of τ_R on the deposition rate at 1100 °C is completely different from that at 50 °C. The surface reaction kinetics being highly activated by the concentration of reactive intermediates and most of all by temperature, the deposition rate is essentially limited by mass transfer, as suggested by the strong increase of R with τ_R (see Fig. 10).

The apparent kinetic constant k for the homogeneous decomposition of VTS was calculated from the changes of the VTS partial pressure (P_{VTS}) versus τ_R using the following equation:

$$\frac{d(P_{VTS})}{d\tau_R} = -k P_{VTS}^a \quad (1)$$

where a is the partial order of reaction. The best fit of the experimental $P(R)$ data was obtained for $a = 1$ (Fig. SI3), suggesting a unimolecular decomposition of VTS (as for MTS). k obeys an Arrhenius law (where E_a is the apparent activation energy)

$$k(T) = A e^{-E_a/RT} \quad (2)$$

By integration of equation (1), with $a = 1$ and P_{VTS}^0 the initial VTS partial pressure, then comes

$$k(T) = \frac{1}{R} \ln\left(\frac{P_{0VTS}}{P_{VTS}}\right) \quad (3)$$

and finally

$$\ln\left(\frac{1}{R} \ln\left(\frac{P_{0VTS}}{P_{VTS}}\right)\right) = \ln(A) - \frac{E_a}{RT} \quad (4)$$

The apparent activation energy E_a of the kinetic constant k can then be obtained from the slope obtained after plotting the left side of equation (4) against $1/T$.

The apparent activation energy of VTS decomposition for $P = 10$ kPa is about $E_a = 280 \pm 10$ kJ.mol⁻¹ for $P = 2$ kPa and 250 ± 50 kJ.mol⁻¹ for $P = 5$ and 10 kPa (Fig. 12).

Finally, the study of the influence of the total flow rate was completed by comparing different couples of $(P; T)$ conditions leading to pure SiC coatings with relatively high and similar deposition rates (Figs. 2,5,8, 9, SI1): 2 kPa – 1025 °C (already examined above, see Fig. 10), 5 kPa – 975 °C and 10 kPa – 900 °C (Fig. 13). R increases slightly with Q_{tot} for the first two conditions, characterizing a limitation by both diffusion and surface reactions. The 10 kPa – 900 °C condition leads to a slightly negative slope of R vs. Q_{tot} , which is related to a chemical reaction regime that is little affected by homogeneous reactions. This condition lies in the high temperature region of the intermediate linear domain, which has been identified in the Arrhenius plot ($T = 800 - 900$ °C) (Fig. 9a, see section 3.2.).

3.4. Influence of VTS dilution

The influence of dilution in H₂ on the deposition kinetics and the decomposition of VTS was investigated at $P = 2$ kPa. In a first step, the influences of the temperature on the deposition rate and the VTS decomposition ratio $(1 - P_{VTS}/P_{VTS,0})$ at different dilution ratios ($a = 10, 20$ and 30)

were compared. The increase of the dilution in H₂ (*i.e.* of α) results in a shift to a lower temperature and a more progressive transition between the low and high temperature kinetic regimes (Fig. 14). The apparent activation energy of the low temperature kinetic regime is also lower, suggesting a change in the deposition mechanism, and the deposition rate in the high temperature regime(s) is also lower. The increase of α simultaneously leads to an increase of VTS decomposition at a given temperature (Fig. 15).

To better dissociate their respective role, the VTS and H₂ apparent partial orders were evaluated at $T = 75\text{ }^{\circ}\text{C}$ and $1000\text{ }^{\circ}\text{C}$, *i.e.* respectively in the low temperature and high temperature kinetic regimes (Fig. 2a). The initial partial pressures of both VTS and H₂ ($P_{\text{H}_2}^0$) were modified independently (at a constant total flow rate of $Q_{\text{tot}} = 205\text{ sccm}$) and their respective influences on the deposition rate and the composition of the gas phase were examined. At $T = 75\text{ }^{\circ}\text{C}$, R does not vary significantly with P_{VTS}^0 between 0.1 kPa and 0.2 kPa (Fig. 16a). The FTIR analysis shows that VTS is simultaneously less decomposed (Fig. 16b). These results are both consistent with those obtained in the study of the influence of α (Figs. 14 and 15). On the other hand, the increase of $P_{\text{H}_2}^0$ has no effect on R over the whole range of partial pressure tested (Fig. 17a), while a higher decomposition of VTS (Fig. 17b) and an increase of the concentration of hydrogen chloride, ethylene and trichlorosilane are detected simultaneously [30]. A similar influence of $P_{\text{H}_2}^0$ was observed on the decomposition of MTS [33]. At $1000\text{ }^{\circ}\text{C}$, in the high temperature regime, the apparent VTS partial order is approximately equal to 2 for $P_{\text{VTS}}^0 = 0.05 - 0.1\text{ kPa}$ (Fig. 16a). It gradually decreases as P_{VTS}^0 increases, down to a negative value at high partial pressures. Unlike at $75\text{ }^{\circ}\text{C}$, the H₂ partial order remains constant and equal to 1.2 at $1000\text{ }^{\circ}\text{C}$ (Fig. 17a). On the other hand, as at $75\text{ }^{\circ}\text{C}$, the decomposition of VTS is limited (respectively promoted) by the raise of P_{VTS} (respectively $P_{\text{H}_2}^0$, Figs. 16b and 17b). No change in the chemical composition of the solid was detected while varying P_{VTS}^0 and $P_{\text{H}_2}^0$ in the above partial orders study, the coating is respectively free carbon-rich and stoichiometric at 75 and $1000\text{ }^{\circ}\text{C}$.

The influence of the nature of the diluent gas was finally evaluated by comparing the deposition kinetics and the decomposition behavior of VTS, when diluted in pure H₂ or pure Ar ($P_{\text{Ar}}^0/P_{\text{VTS}}^0 = 13$, $P = 2\text{ kPa}$ and $Q_{\text{tot}} = 150\text{ sccm}$). The deposition rate is typically two orders of magnitude lower for VTS/Ar than for VTS/H₂ and obeys an Arrhenius law with an apparent activation energy of about 250 kJmol^{-1} over the range $1025 - 1125\text{ }^{\circ}\text{C}$ (R could not be measured below $1025\text{ }^{\circ}\text{C}$ with

argon, compared to 25 °C with H₂, Fig. 18a). The FTIR analysis shows in parallel that VTS is less decomposed with Ar, compared to H₂, while the formation of less hydrogenated gas species like C₂H₂ and SiCl₄ is favored (Fig. 18b). The Raman and EDS analyses of the coating obtained with Ar show that it consists of nearly pure carbon for the whole temperature domain. Similar results were obtained from studies by Kim *et al.* on MTS/Ar mixtures [34]. These authors indeed reported a decrease of the growth rate and a carbon enrichment in the deposit for temperatures below 1150 °C. The CVD from VTS diluted in argon thus presents many similarities with the CVD in H₂ in the low temperature kinetic regime.

3.5. Influence of the addition of gas products in the initial VTS/H₂ mixture

In order to better understand the influence of the main products formed in the gas phase at $P = 2$ kPa, the SiHCl₃ (TCS), C₂H₄ and C₂H₂ apparent partial orders were evaluated at $T = 975$ °C and 1000 °C and the nature of the resulting deposit was examined. As above for VTS, the initial partial pressures of the three gaseous species were modified ($Q_{tot} = 205$ sccm) and their influences on the deposition rate and the composition of the deposit were examined. The change in the initial partial pressure of SiHCl₃, P_{TCS}^0 , does not significantly affect R at both temperatures within the P_{TCS}^0 domain explored (Fig. 19a). R is however lower at $T = 1000$ °C than without SiHCl₃ addition. Whereas the deposited solid remains carbon-rich at $T = 975$ °C, it consists of pure SiC at $T = 1000$ °C for all P_{TCS}^0 tested.

R also does not vary much with $P_{C_2H_4}^0$ for both temperatures. However, an inhibition effect is also observed at $T = 1000$ °C after the addition of C₂H₄ (Fig. 19b). As for TCS, the apparent partial order is low but could not be determined precisely due to too much uncertainty on R . The obtained deposit being too thin, EPMA or EDS analyses could not be performed. Yet, Raman spectroscopy measurements evidenced that excess carbon was formed for both temperatures after C₂H₄ addition.

Unlike for the other two gases, R increases significantly with $P_{C_2H_2}^0$, with an apparent partial order approximately equal to 1 for both temperatures (Fig. 19c). The deposition rate is again inhibited at 1000 °C at low values of $P_{C_2H_2}^0$. As after adding C₂H₂, the Raman spectroscopy analyses reveal the presence of a large amount of free carbon in the deposit.

3.6 Infiltration capability of VTS

The porous structure of the fibrous fabrics used to produce SiC/SiC composites is particularly complex and multiscale, so that its infiltration is in practice difficult to characterize. Model porous substrates were therefore preferred to evaluate the infiltration capability of the VTS precursor in various CVD conditions. Open pores, with openings of about 100 μm or a few hundred microns, were chosen because they are representative of the macropores of SiC/SiC composites. Their infiltration capacity is crucial, as many of them are interconnected and communicate with the rest of the smaller pores. Straight parallelepipedic 20 mm-long channels with narrow slit-shaped openings of various widths at both ends were used as model pores. These substrates consisted in two tightly-assembled graphite plates, the first one with three trenches of equal width (2 mm) and different depths (50, 100 and 300 μm) machined on one side, the second one being completely flat (Fig. 20). The porous substrates were installed at the same place as the dense substrates used for the kinetic study, the channels being perpendicular – the openings parallel – to the gas flow direction.

The deposition rate was normalized with respect to the maximum value (generally reached at the surface) for an easier comparison of pore depth profiles. Under a given CVD condition (*e.g.* here $T = 1025\text{ }^\circ\text{C}$, $P = 2\text{ kPa}$, $\lambda = 13$ and $Q_{\text{tot}} = 300\text{ sccm}$), the larger the opening width, the easier the diffusion of the gases inside the pore, and the better the infiltration (Fig. 21).

Since the deposition temperature was found to induce important changes in the deposition rate and the composition of the solid and the gas phase, different infiltration tests were achieved at various T and constant pressure ($P = 2\text{ kPa}$), dilution ratio in H_2 ($\lambda = 13$) and total flow rate ($Q_{\text{tot}} = 300\text{ sccm}$). The resulting infiltration profiles for a 300 μm -wide pore are shown in Fig. 22. The infiltration test carried out at $T = 50\text{ }^\circ\text{C}$ leads to a remarkable result: the coating is very thin and consists of nearly pure carbon at the outside of the substrate and near the entrance in the channel, and turns to pure SiC at a distance of 0.6 mm and deeper into the pore. The transition from the carbon-rich deposit to pure SiC is abrupt and associated with a sharp increase of the deposition rate. The maximum value reached at 4.6 mm is $2.8\text{ mm}\cdot\text{h}^{-1}$ whereas the value at the surface is only

0.06 mm.h^{-1} . This phenomenon can be likely related to the kinetic transition observed during the CVD experiments carried out while raising T in the range 50 – 1000 °C. Contrary to the 50 °C experiment, the infiltration tests performed at 1025 and 1100 °C lead to pure SiC at the surface and inside the pore. On the other hand, the deposition rate suddenly drops to nearly zero within a short distance (< 1 mm) of the pore entrance (Fig. 22). The maximum values reached at the surface are respectively 16 and 15 mm.h^{-1} (a slight gas depletion probably reduces the deposition rate at high temperature).

4. Discussion

4.1. The low temperature regime: CRR1

The low temperature chemical reaction regime observed using the VTS/H₂ system (it will be referred to as CRR1 in the following) corresponds to the starting decomposition of VTS (Fig. 2b). It is associated to the deposition of large excess of carbon (Fig. 5) at low deposition rates (Fig. 2a), with an apparent activation energy of about 250 kJ.mol^{-1} (Fig. 10). Some similar features have also been encountered for the VTS/Ar system. Indeed, in this case R is low, its apparent activation energy is similar (Figs. 18a) and the deposit is carbon-rich, although formed at a much higher temperature than for a dilution in H₂. Besides, the gas phase analysis reveals that the decomposition of VTS occurs at a higher temperature (Fig. 18b) and with a more thermally activated process ($E_a = 350 \text{ kJ.mol}^{-1}$ versus 280 kJ.mol^{-1} for VTS/H₂ in the CRR1 regime, Fig. 18a). This result thus suggests that the decomposition reaction of VTS might not be the same for the VTS/H₂ and VTS/Ar systems. A similar behavior was also reported by one of us during a study of the SiHCl₃/C₂H₂/H₂ system [35]. The deposition rate and the apparent activation energy obtained in this case were indeed very close to those of the CRR1 regime for the VTS/H₂ system. The coating then was also deposited at low temperature and rich in free carbon, supposedly controlled by the adsorption of C₂H₂ due to its high sticking coefficient. Although the decomposition steps obviously vary for these various precursor systems, the nature of the solid, the deposition rate and the apparent activation energy are all rather similar. Such common features suggest that the

limiting stage of CRR1 regime may be related to chemical reactions involving unsaturated hydrocarbon species.

Given the nature the hydrocarbons detected by FTIR from the VTS/H₂, VTS/Ar and SiHCl₃/C₂H₂/H₂ systems [35], it can be assumed that three major unsaturated species could participate in the deposition of free carbon. C₂H₂ is produced in low amounts in the CRR1 regime from VTS/H₂ and in larger proportions from VTS/Ar (Figs. 2 and 18). Its sticking coefficient is of the order of 0.02 – 0.05 [36–39] and its addition to the VTS/H₂ mixture increases significantly the deposition rate in the CRR1 regime (Fig. 19c). López-Honorato *et al.* also reported that a thin carbon layer was deposited above the fluidized bed (FB) in a FB-CVD reactor using a MTS/C₂H₂/H₂ mixture, while a pure SiC coating was grown on the FB particles themselves [40]. In comparison, no such carbon layer was produced using MTS/H₂ or MTS/C₃H₈/H₂ mixtures in the same conditions, suggesting that C₂H₂ plays a major role in the deposition of free carbon. C₂H₄ is found in large amounts in the gas phase for the VTS/H₂ system in the CRR1 regime (Figs. 2). Its sticking coefficient is about ten times lower than that of C₂H₂ [37,38] and its addition in the gas does not increase of the deposition rate (Fig. 19b). We did not observe the formation of carbon-rich coating using a SiHCl₃/C₂H₄/H₂ mixture, at $P = 2$ kPa, at the temperatures at which the deposit starts to be formed [35]. On the other hand, Sotirchos *et al.* noticed that the addition of C₂H₄ in a mixture of MTS/H₂ improved the deposition rate of free carbon at $P = 13.3$ kPa and $T = 1075$ °C [17]. But this result could be due to larger concentrations of C₂H₂ and C₂H₃, resulting from the decomposition of C₂H₄, possibly related to the high pressure applied in comparison with that used by us ($P = 2$ kPa). We indeed did not detect C₂H₂ by FTIR from the SiHCl₃/C₂H₄/H₂ mixture. Finally, the radical C₂H₃ can be produced by the scission of the Si–C bond of VTS. This species is likely at the origin of C₂H₂ and C₂H₄, detected by FTIR. It has a sticking coefficient similar to that of C₂H₂ and could thus be involved in the deposition of free carbon [37,38].

The apparent activation energies reported for the CVD of pyrolytic carbon from C₂H₂ and C₂H₄, at atmospheric pressure, are respectively 138 and 155 kJmol⁻¹ [41], which is much less than the 250 kJmol⁻¹ found for the CRR1 regime. The respective deposition mechanisms of carbon are obviously distinct, probably due to the very different pressure. The presence of chlorosilicon species could also promote another deposition mechanism. Sotirchos *et al.* indeed noticed an increase of the deposition rate of pyrolytic carbon from C₂H₄/H₂ in presence of MTS [17]. These authors explained this phenomenon by a reaction between CH and SiCl₃ species adsorbed on two

adjacent sites to incorporate a carbon atom in the coating and form adsorbed SiCl_2 and HCl . Yet, this purely heterogeneous model is not able to explain the growth of almost pure carbon under steady state conditions. The increase in deposition rate can be more likely explained by the occurrence of radical reactions related to the chlorine chemistry. The appearance of Cl radicals in the gas phase indeed lead to the formation of highly reactive hydrocarbon species, such as CH_3 , which may serve as effective precursors of carbon [42,43]. We also showed that the reactional mechanism involved in the hydrocarbon gas phase produced from the $\text{SiHCl}_3/\text{C}_2\text{H}_4/\text{H}_2$ system is linked to that governing the chlorosilicon homogeneous phase via the radical H . H is indeed formed from reactions between hydrocarbons, and consumed through reactions between chlorosilicon species, thus modifying the balance between the two chemical systems [35].

4.2. The C / SiC transition and the hysteresis phenomenon

From VTS/H_2 , at $P = 2$ kPa, the increase of the deposition temperature between 975 and 1000°C results in the transition between a carbon-rich coating (in the CRR1 regime) to a pure SiC coating, whose deposition is controlled by a distinct – high temperature – chemical reaction regime (referred to as CRR2) (Fig. 5). A very similar phenomenon was observed between 1000 and 1025 °C using a $\text{SiHCl}_3/\text{C}_2\text{H}_2/\text{H}_2$ mixture (also at $P = 2$ kPa), with an initial C/Si ratio in the gas phase of 3 [35]. This transition can be explained by a change in the nature of the chlorosilicon gas phase at high temperature, promoting the formation SiCl_2 as a precursor of silicon. The origin of this transition for the VTS/H_2 system is probably more complex considering the hysteresis of the deposition rate during the temperature rise or fall observed between CRR1 and CRR2 at $P = 5$ kPa (Fig. 8a). A hysteresis is indeed also observed at 10 kPa, but between CRR1 and an intermediate regime below CRR2, referred to as CRR2* (Fig. 9a). In the VTS case, the hysteresis seems more likely related to a heterogeneous process. This assumption is supported by the fact that the changes in the gas phase are not themselves subject to hysteresis upon heating/cooling. Sotirchos *et al.* reported a very similar hysteresis in both R and deposit composition with a $\text{MTS}/\text{C}_2\text{H}_4/\text{HCl}/\text{H}_2$ mixture [17,44–46]. These authors correlated this phenomenon to modifications of both the deposition temperature and the initial HCl concentration in the gas phase, and explain it by the existence of a multiplicity of steady states in the co-deposition of SiC and C for a given experimental condition. This work also showed that the formation of free carbon, following the

increase in C_2H_4 concentration, is accompanied by a sharp drop of the deposition rate [17,44–46]. This result is very similar to that reported here at $T = 1000$ °C, after the addition of 0.025 mol. % of C_2H_2 or C_2H_4 to the initial VTS/ H_2 mixture (Fig. 19b,c). Sotirchos *et al.* suggested that the sp^2 -C deposit inhibits the deposition of SiC, the transition from C to SiC being controlled by the interaction between the heterogeneous mechanisms of deposition the two respective phases. The model describing the hysteresis phenomenon involves a competition between the different adsorption sites of $SiCl_2$ and C_2H_4 .

On the basis of the model suggested by Sotirchos *et al.* and the current results, three major effects could explain the hysteresis phenomenon.

4.2.1. the role of HCl

In their study of the MTS/ C_2H_4 / H_2 system, Sotirchos *et al.* noticed that (i) no hysteresis appeared without HCl addition and (ii) the addition of more than 10 mol. % HCl induced a strong drop of the deposition rate. The latter effect is due to the inhibition of the silicon adsorption sites by chlorine blockage [13]. It has often been mentioned in CVD studies of the MTS/ H_2 system [8,9,12,29] and described by modelling [47]. It could also explain the decrease of the deposition rate observed in the CRR2 regime (at $T = 1000$ °C) after the addition of $SiHCl_3$ in the VTS/ H_2 mixture (Fig. 19a). Not only can the adsorption of silicon be hindered by HCl, but chlorine could also enhance the deposition of carbon via radical reactions in the CRR1 regime (see section 4.1).

As the temperature rises from an initial low T level, the silicon sites, saturated by chlorine, inhibit the SiC deposition at the surface [48]. Simultaneously, the reactive hydrocarbon gas phase (containing C_2H_2 and C_2H_3) contributes to the deposition of free carbon at low deposition rate. Conversely, as the temperature decreases from an initial high level, the Si sites are free of chlorine that has desorbed at high temperature, and the SiC deposit is free to form at high deposition rate. The consecutive of rise and fall of deposition temperature thus induce the hysteresis of the deposition rate and the deposit composition. The presence of chlorine and silicon trapped in the free carbon network of the coating obtained in the CRR1 regime (see section 3.1.) is also consistent with such a mechanism. The fact that the hysteresis appears only at $P = 5$ kPa could be then related to the larger amounts of HCl produced at high pressure, as suggested by FTIR analyses [30].

In addition to the influence of HCl, the role of the hydrocarbon gas phase is also decisive for the appearance of the above hysteresis phenomenon. Indeed, no hysteresis was found for the

MTS/HCl/H₂ system: Sotirchos *et al.* observed it only within a narrow C₂H₄ partial pressure range. A highly reactive hydrocarbon phase is essential, but so is the formation of the solid free carbon phase, as discussed below.

4.2.2. *The chemical nature of the surface of the deposit*

The sticking coefficient of chlorosilicon species is probably much lower on the free carbon phase than on the SiC phase, due to the different surface atomic configurations. The growth of hexagonal carbon layers at the expense of SiC, during the CRR1 regime, is therefore expected to hinder the adsorption of chlorosilicon species. Hence, the different chemical nature of the deposit surface encountered either on heating or cooling could obviously contribute to the hysteresis of the deposition rate of pure SiC and the sp² carbon-rich material.

4.2.3. *The nature of the effective precursors of the deposit*

Sukkaew *et al.* established by *ab initio* calculation that contrary to CH₃ or C₂H₄, which is cleaved in two distinct CH_x groups, C₂H₂ is adsorbed at the (0001) surface, Si face, of 4H-SiC in a configuration such that its two carbon atoms remain chemically bonded [39]. Similar conclusions had been drawn by Di Felice *et al.* who studied C₂H₂ adsorption on both Si(111) and (Si(001) surfaces of 3C-SiC [49]. It is then reasonable to assume that a Si surface of SiC saturated by adsorbed C₂H₂ can evolve towards a continuous sp² carbon surface by dehydrogenation and atomic reorganization. Although none of these authors considered the presence of chlorine in the system, Di Felice *et al.* suggested that the stability of the C-C bond after C₂H₂ adsorption could lead to an inhibition of the SiC growth. In the present case, the adsorption of SiCl₃, the precursor of SiHCl₃ detected at the reactor outlet, should therefore be more difficult at a site where C₂H₂ is adsorbed – and *a fortiori* at a sp² carbon surface – than at sites where CH₃ or C₂H₄ are adsorbed. Even though the real nature of the surface is obviously different from that considered by Di Felice *et al.* or Sukkaew *et al.*, these *ab initio* studies tend to show that the free carbon phase growth in the low temperature CRR1 regime could result from a preferential adsorption of C₂H₂. At higher temperature, the formation of another hydrocarbon species able to form sp³ Si-CH_x bonds on a Si surface of SiC (contrary to C₂H₂) – or another chlorosilicon species able to form sp³ C-SiCl_x bonds

on a sp^2 carbon surface – could be at the origin of the transition from carbon rich to pure SiC coating. The C_2H_4 concentration was found to significantly increase with T over the CRR1 domain (Figs. 2b,8b,9b). This species could contribute to the incorporation of increasing amounts of sp^3 carbon atoms over the CRR1-CRR2 transition and thus the formation of SiC. Its particular adsorption configuration promotes surface reaction with chlorosilicon species [39,49].

4.3. The different kinetic regimes

The Arrhenius plots of the deposition rate for the MTS/ H_2 , SiHCl₃/ C_2H_4/H_2 and VTS/ H_2 systems are compared in Fig. 23 ($P = 2$ kPa, MTS/ H_2 : $Q_{H_2}/Q_{MTS} = 10$, $Q_{tot} = 200$ sccm [35], SiHCl₃/ C_2H_4/H_2 : $Q_{H_2}/Q_{SiHCl_3} = 10$, $Q_{C_2H_4}/Q_{SiHCl_3} = 3/2$, $Q_{tot} = 250$ sccm [35], VTS/ H_2 : see Fig. 2a).

The CRR1 regime observed for $T < 975$ °C is a specificity of the VTS/ H_2 systems. It is kinetically controlled, probably by the surface reaction of C_2H_2 that is produced in the gas phase (see section 4.2.3), and it leads to the growth of carbon-rich material at low deposition rate. The activation energy is about 250 kJmol⁻¹ and the apparent C_2H_2 partial order of about 1 (Fig. 19c).

For $T > 1000$ °C, in the CRR2 regime, the thermal behavior of R for the VTS/ H_2 system is very similar to that for the MTS/ H_2 and SiHCl₃/ C_2H_4/H_2 systems. The apparent activation energy at $T = 1000 - 1050$ °C is close for the three systems (150 ± 10 kJ.mol⁻¹), suggesting that similar heterogeneous reactions are kinetically limiting for the various precursors [7,32,35]. The main effective silicon precursors are likely similar for all three systems, *i.e.* SiCl₂ and SiCl₃ [5,7,50], which is probably not the case for the hydrocarbon precursors. For MTS/ H_2 , CH₃ is more likely the major carbon precursor [5,7,50], while it is more probably C_2H_2 or C_2H_3 for the SiHCl₃/ C_2H_4/H_2 [35] and VTS/ H_2 system.

As observed here for the VTS/ H_2 system, increasing the pressure in the MTS/ H_2 system sometimes give rise to a new intermediate kinetic regime between the CRR/MTR transition, referred to as “third sub-domain” or CRR3, and a shift towards low temperatures of the kinetic transition between the *CRR1* and the *CRR2* regime [32] (it is important to mention that *CRR1* and *CRR2* regimes, here written in italic and reported in [32] for the MTS/ H_2 system, have nothing in common with the CRR1 and CCR2 regimes described in the present study on the VTS/ H_2 system). The high

pressure *CRR3* domain was associated to a change in the heterogeneous mechanism, associated to the formation of large amounts of HCl inhibiting the SiC growth [32]. The intermediate *CRR2** domain observed at $P = 10$ kPa for VTS/H₂ (Fig. 9a) probably has a different origin from that of *CRR3* for MTS/H₂. R was indeed found to decrease when Q_{tot} increases, in the *CRR2** domain (at $P = 10$ kPa and $T = 900^\circ\text{C}$, Fig. 13), suggesting a lower decomposition of VTS due to insufficient residence time (a strong decrease of the VTS decomposition was indeed detected in parallel by FTIR) [30]. Moreover, the apparent activation energies of the deposition rate in the *CRR2** domain (Fig. 9a) is close to that of the VTS homogeneous decomposition (Fig. 12), suggesting that R is likely limited by the latter reaction in this particular regime. The shift towards low temperatures of the kinetic transitions, observed when P increases (Figs. 2a,8a,9a,SI1), is due to an increase of both the molecular collision probability and the residence time, these effects both promoting the VTS decomposition Figs. 2b,8b,9b,11).

In the highest temperature range (*i.e.* beyond the *CRR2* regime), at $P = 2$ and 5 kPa, the kinetic rate becomes increasingly controlled by mass transfers (Figs. 2a,8a,10) and all the partial pressures of the gas product decrease as T increases, except HCl and C₂H₂ (Figs. 2b,8b). In parallel, free carbon is co-deposited at the highest temperatures of this regime, similarly as observed for SiHCl₃/C₃H₈/H₂ and SiHCl₃/C₂H₄/H₂ [35]. This carbon enrichment of the coating seems related to a depletion of the gas phase in chlorosilicon species participating to the deposition silicon (Fig. 7a) and to the formation of highly reactive hydrocarbons (*e.g.* C₂H₂ or heavier species).

4.4. Relationship between CVD and infiltration conditions

At $P = 2$ kPa and $T = 950^\circ\text{C}$, *i.e.* in the *CRR1* deposition domain, the infiltration test leads to strong discontinuities along the longitudinal deposition profile. The deposition rate is indeed very low and the deposit carbon-rich for $x < 0.6$ mm, whereas R increases abruptly and the coating turns to pure SiC for $x > 0.6$ mm (Figs. 22). This infiltration behavior is obviously very different from what is generally observed for other precursors, in particular for the MTS/H₂ system (see in Fig. 24 an example of infiltration profile recorded for $T = 970^\circ\text{C}$, $Q_{H_2}/Q_{MTS} = 3$, $Q_{tot} = 160$ sccm). The sudden transition in both R and solid composition for the VTS/H₂ system can be assigned to a local change of the effective precursor of the deposit. Outside and near the pore entrance, where nearly pure CVD conditions apply, the deposition of a carbon-rich coating at very low deposition rates

could be closely related to the formation of C_2H_2 in the gas phase and its adsorption at the surface of the deposit (see section 4.2.3.). The depletion of C_2H_2 consumed by the free carbon deposition at the entrance of pore and the increase of the local residence time (as suggested by Fig. 11a) would then lead, deeper in the pore, to an increase of the concentration of C_2H_4 . The latter species is capable of adsorbing to the surface and disrupting the deposition of sp^2 carbon (see section 4.2.3.). The structural disorder of the free carbon phase increasing, the $SiCl_2$ adsorption would then become more favorable and thus promote the deposition of pure SiC at high deposition rates. Hence, the increase in the concentration of C_2H_4 and $SiCl_2$ (caused respectively by the C_2H_2 depletion and increase of r) from the outside to the inside of the pore, would be responsible for the carbon-rich to pure SiC transition and the remarkable increase of the deposition rate. This hypothesis is similar to that made by Wang and Tsai to explain the transition from a carbon-rich to a silicon-rich deposit, between the reactor inlet and outlet, using $SiH_2Cl_2/C_2H_2/H_2$, [51].

The carbon-rich to SiC transition observed at 950 °C for the VTS/ H_2 system could be problematic for specific applications. Another potential way to improve the stoichiometry and homogeneity of infiltrated deposits could be the use of two separate silicon and carbon precursors of appropriate reactivity. We have also explored this approach (see in Fig. 24 an example of infiltration profile recorded using a $SiHCl_3/C_3H_8/H_2$ mixture, for $T = 970^\circ C$, $Q_{H_2}/Q_{SiHCl_3} = 10$, $Q_{C_3H_8}/Q_{SiHCl_3} = 1$, $Q_{tot} = 240$ sccm), which we will discuss in a forthcoming article.

5. Conclusions

The deposition of SiC from vinyltrichlorosilane was investigated in terms of deposition rate, chemical composition of the solid and nature of the gas phase at the exhaust of a hot-wall reactor. Three different domains of deposition rate were observed and associated to different sets of homogeneous and heterogeneous reactions

- At low temperature a CRR1 domain with an activation energy of $230 \text{ kJ}\cdot\text{mol}^{-1}$ is observed. The deposit consists mainly of carbon with a only few percent of silicon. VTS tends to decompose into highly reactive carbon-bearing species such as C_2H_2 , in contrast with the CH_3 radicals formed from MTS.

- At medium temperature, pure SiC is deposited within the CRR2 domain ($E_a = 150 \text{ kJ.mol}^{-1}$) beyond a narrow domain of bistability. Ethylene and SiCl₄ are respectively the major carbon and silicon-bearing species detected in the CRR2 domain, while the concentration of SiHCl₃ is significantly reduced.

- At high temperature, mass transfer becomes the limiting step of the deposition rate. SiC is obtained with a small excess of carbon due to the formation of highly reactive hydrocarbons (associated with a higher concentration of C₂H₂ in the gas phase) and depletion of silicon species.

The domain of bistability observed between the CRR1 and CRR2 regime, is related to a hysteresis of the deposition rate upon the temperature increase or decrease. This effect is assigned to a change in the nature of the deposit (from a carbon-rich to a pure SiC coating) affecting the heterogeneous reactions.

The pressure dependence of the deposition rate allowed to establish a P-T diagram delimiting the different kinetic and composition domains for the SiC deposition from VTS (Fig. 14).

The rate constant and the apparent activation energy of the unimolecular decomposition of VTS ($E_a = 230 \text{ kJ.mol}^{-1}$) were determined from FTIR analyses performed as a function of the residence time τ_R . The increase of τ_R leads to a higher VTS decomposition rate and therefore a higher deposition rate, particularly in the MTR domain.

The nature of the dilution gas and the dilution ratio of VTS was varied in order to understand the role of hydrogen in the decomposition of the precursor and help proposing a homogeneous chemical mechanism. Although the coating consists mainly of carbon when using Ar as the diluent gas, pure SiC was deposited at all the initial partial pressures of H₂ and VTS examined for the VTS-H₂ system in the CRR2 domain.

The infiltration of pure SiC in model channel pores is more homogeneous when decreasing the substrate temperature, although no SiC is deposited at the entrance of the pores at the lowest temperatures ($T = 50^\circ\text{C}$).

Acknowledgements

The authors acknowledge Safran Ceramics, the French National Association for Research and Technology (ANRT, CIFRE contract N° 2015/1426) and the Claude Delhorme Research Center from Air Liquide for their help and financial support. They also gratefully thank A. Delcamp, C. Descamps and S. Goujard from Safran Ceramics, as well as T. Renault and C. Dussarat from Air Liquide, for regular and fruitful discussions.

CRedit author statement

A. Desenfant: Methodology, Investigation, Data curation, Visualization, Writing - Original draft preparation, **G. Laduye:** Methodology, Writing - Reviewing and Editing, **G. L. Vignoles:** Writing - Reviewing and Editing, **G. Chollon:** Methodology, Writing - Reviewing and Editing, Supervision.

References

- [1] R. Naslain, SiC-Matrix Composites μ Nonbrittle Ceramics for Thermo-Structural Application. *Int. J. App. Ceram. Technol.* 2 (2005) 5-84. <https://doi.org/10.1111/j.1744-7402.2005.0200 .x>
- [2] F. Christin, Design, Fabrication, and Application of Thermostructural Composites (TSC) like C/C, C/SiC, and SiC/SiC Composites, *Adv. Eng. Mater.* 4 (2002) 03- 12. <https://doi.org/10.1002/adem.2002 0001>
- [3] J. Lamon, Chemical Vapor Infiltrated SiC/SiC Composites (CVI SiC/SiC), in *Handbook of Ceramic Composites*, N.P. Bansal ed., Springer, Boston, USA, 2005, pp.55-76. https://doi.org/10.1007/0-387-23 86-3_3
- [4] F. Loumagne, F. Langlais, R. Naslain, S. Schamm, D. Dornignac, J. Sévely, Physicochemical properties of SiC-based ceramics deposited by low pressure chemical vapor deposition from CH₃SiCl₃-H₂, *Thin Solid Films* 254 (1 5) 75-82. [https://doi.org/10.1016/0040-60 0\(4\)06237-F](https://doi.org/10.1016/0040-60 0(4)06237-F)
- [5] W. G. Zhang, K. J. Hüttinger, CVD of SiC from Methyltrichlorosilane. Part II μ Composition of the Gas Phase and the Deposit. *Chemical Vapor Deposition*, 7 (2001) 173-181. [https://doi.org/10.1002/1521-3862\(200107\)7:4<173: AID-CVDE173>3.0.CO;2-X](https://doi.org/10.1002/1521-3862(200107)7:4<173: AID-CVDE173>3.0.CO;2-X)

- [6] J. A. DiCarlo, Advances in SiC/SiC Composites for Aero Propulsion, Chap. 7 of “Ceramic Matrix Composites”, N. P. Bansal & J. Lamon eds., Wiley-American Ceramic Society, 2014, pp. 217-235. https://dx.doi.org/10.1002/781118832_8.ch7
- [7] F. Loumagne, F. Langlais, R. Naslain, Reactional mechanisms of the chemical vapour deposition of SiC-based ceramics from CH₃SiCl₃/H₂ gas precursor, J. Cryst. Growth 155 (1-5) 205-213. [https://doi.org/10.1016/0022-0248\(95\)00181-6](https://doi.org/10.1016/0022-0248(95)00181-6)
- [8] Y. Yang, W.-G. Zhang, Chemical vapor deposition of SiC at different molar ratios of hydrogen to methyltrichlorosilane, J. Central South Univ. Technol. 16 (2003) 0730-0737. <https://doi.org/10.1007/s11771-003-0121-4>
- [9] G.D. Papasouliotis, S.V. Sotirchos, Experimental study of atmospheric pressure chemical vapor deposition of silicon carbide from methyltrichlorosilane, J. Mater. Res. 14 [8] (1999) 337-340. <https://doi.org/10.1557/JMR.1999.0460>
- [10] A. Josiek, F. Langlais, X. Bourrat, A study of the transition between growth of stoichiometric and silicon-excess silicon carbide by CVD in the system MTS/H₂, Chemical Vapor Deposition 2 (1-6) 17-21. <https://doi.org/10.1002/cvde.160020105>
- [11] G. Papasouliotis, S. Sotirchos, Hydrogen chloride effects on the CVD of silicon carbide from methyltrichlorosilane, Chemical Vapor Deposition, 4 (1-8) 235-246. [https://doi.org/10.1002/\(SICI\)1521-3862\(199804\)04:06<235::AID-CVDE235>3.0.CO;2-R](https://doi.org/10.1002/(SICI)1521-3862(199804)04:06<235::AID-CVDE235>3.0.CO;2-R)
- [12] D. Lespiaux, F. Langlais, R. Naslain, S. Schamm, J. Sévely, Chlorine and Oxygen Inhibition Effects in the Deposition of SiC-based Ceramics from the Si-C-H-Cl system, J. Eur. Ceram. Soc. 15 (1-5) 81-88. [https://doi.org/10.1016/0955-2211\(95\)1303-6](https://doi.org/10.1016/0955-2211(95)1303-6)
- [13] M.T. Schulberg, M.D. Allendorf, D.A. Outka, The interaction of HCl with polycrystalline SiC: evidence for a site-blocking mechanism for HCl inhibition of SiC CVD, MRS Proceedings, Volume 410 (Symposium S – Covalent Ceramics III-Science and Technology of Non-Oxides), G.S. Fischman, A.F. Hepp, A.E. Kaloyeros, P.N. Kumta, J.J. Sullivan eds., 1995, pp. 471-476. <https://doi.org/10.1557/PROC-410-471>
- [14] D. H. Kuo, D. J. Cheng, W. J. Shyy, M.H. Hon, The effect of CH₄ on CVD SiC Growth, J. Electrochem. Soc. 137 (1-0) 3688-3692. <https://doi.org/10.1149/1.2086288>

- [15] B. J. Choi, S. H. Jeun, D. R. Kim, The Effects of C₃H₈ on the Chemical Vapor Deposition of Silicon Carbide in the CH₃SiCl₃ + H₂ System, *J. Eur. Ceram. Soc.* (1 2) 357-363. [https://doi.org/10.1016/055-221\(2\)004-T](https://doi.org/10.1016/055-221(2)004-T)
- [16] J. I. Kim, W. J. Kim, D. J. Choi, J. Y. Park, Deposition of compositionally graded SiC/C layers on C-C composites by low pressure chemical vapor deposition, *J. Nucl. Mater.* 307-311 (2002) 1084-1087. [https://doi.org/10.1016/S0022-3115\(02\)0048-0](https://doi.org/10.1016/S0022-3115(02)0048-0)
- [17] S. V. Sotirchos, I. M. Kostjulin, SiC and C codeposition from CH₃SiCl₃-C₂H₄ mixtures. Proceedings of the 13th International Conference of Chemical Vapor Deposition, T.M. Besmann, M.D. Allendorf, Mc.D. Robinson, R.K. Ulrich eds., Electrochemical Society Proceedings, Vol. 6-5, 1 6, pp. 733-738.
- [18] T. Noda, H. Araki, F. Abe, M. Okada, Microstructure and mechanical properties of CVI carbon fiber/ SiC composites, *J. Nucl. Mater.* 1 1-1 4 (1 2) 53 -543. [https://doi.org/10.1016/S0022-3115\(02\)80103-7](https://doi.org/10.1016/S0022-3115(02)80103-7)
- [19] H. Araki, T. Noda, W. Yang, A. Kohyama, Homogeneity and flexural properties of SiC/SiC composites prepared by CVI method, *J. Nucl. Mater.* 307-311 (2002) 1210-1214. [https://doi.org/10.1016/S0022-3115\(02\)01061-7](https://doi.org/10.1016/S0022-3115(02)01061-7)
- [20] T. Taguchi, N. Igawa, R. Yamada, S. Jitsukawa, Effect of thick SiC interphase layers on microstructure, mechanical and thermal properties of reaction-bonded SiC/SiC composites, *J. Phys. Chem. Solids.* 66 (2005) 576-580. <https://doi.org/10.1016/j.jpcs.2004.06.034>
- [21] W. Yang, H. Araki, A. Kohyama, H. Suzuki, T. Noda, ETS-synthesized Hi-Nicalon fiber-SiC matrix composite, *Ceram. Int.* 31 (2005) 47-52. <https://doi.org/10.1016/j.ceramint.2004.03.033>
- [22] A. Saigal, N. Das, Effect of deposition parameters on the strength of CVD beta-SiC coatings, *Adv. Ceram. Mater.* 3 (1 88) 580-583. <https://doi.org/10.1111/j.1551216.188.tb00282.x>
- [23] D. E. Cagliostro, S. R. Riccitiello, M. G. Carswell, Analysis of the pyrolysis products of dimethyldichlorosilane in the chemical vapor deposition of silicon carbide in argon, *J. Am. Ceram. Soc.* 73 (1 0) 607-614. <https://doi.org/10.1111/j.1151-2161.0.tb06560.x>

- [24] D. E. Cagliostro, S. R. Riccitiello, Model for the Formation of Silicon Carbide from the Pyrolysis of Dichlorodimethylsilane in Hydrogen, *J. Am. Ceram. Soc.* 76 (1-3) 3-48. <https://doi.org/10.1111/j.1151-2161.13.tb03688.x>
- [25] D. E. Cagliostro, S. R. Riccitiello, J. Ren, F. Zaghi, Comparison of the Pyrolysis Products of Dichlorodimethylsilane in the Chemical Vapor Deposition of Silicon Carbide on Silica in Hydrogen or Argon, *J. Am. Ceram. Soc.* 77 (1-3) 2721-2726. <https://doi.org/10.1111/j.1151-2161.14.tb04667.x>
- [26] M. S. Cho, J. W. Kim, G. Y. Chung, Manufacturing of ceramic composites reinforced with layered woven fabrics by CVI of SiC from dichlorodimethylsilane. *Korean J. Chem. Eng.* 13 (1-6) 515-521. <https://doi.org/10.1007/BF02706003>
- [27] B. J. Choi, D. W. Park, D. R. Kim, Chemical vapour deposition of silicon carbide by pyrolysis of methylchlorosilanes, *J. Mater. Sci. Lett.* 16 (1-7) 33-36. <https://doi.org/10.1023/A:1018584330520>
- [28] T. Takeuchi, Y. Egashira, T. Osawa, H. Komiyama, A Kinetic Study of the Chemical Vapor Deposition of Silicon Carbide from Dichlorodimethylsilane Precursors, *J. Electrochem. Soc.* 145 (1-8) 1277-1284. <https://doi.org/10.1149/1.1838451>
- [29] W. G. Zhang, K. J. Hüttinger, CVD of SiC from Methyltrichlorosilane. Part I: Deposition Rates, *Chemical Vapor Deposition*, 7 (2001) 167-172. [https://doi.org/10.1002/1521-3862\(200107\)7:4<167::AID-CVDE167>3.0.CO;2-L](https://doi.org/10.1002/1521-3862(200107)7:4<167::AID-CVDE167>3.0.CO;2-L)
- [30] A. Desenfant, Dépôt chimique en phase vapeur (CVD) de carbure de silicium (SiC) à partir de vinyltrichlorosilane (VTS) et de méthylsilane (MS), PhD Thesis, University of Bordeaux, 2018. <https://tel.archives-ouvertes.fr/tel-02078783>
- [31] B. Reznik, H. U. Hüttinger, On the terminology for pyrolytic carbon, *Carbon* 40 (2002) 621-624.
- [32] F. Loumagne, F. Langlais, R. Naslain, Experimental kinetic study of the chemical vapour deposition of SiC-based ceramics from CH₃SiCl₃/H₂ gas precursor, *J. Cryst. Growth* 155 (1-5) 18-204. [https://doi.org/10.1016/0022-0248\(95\)00180-8](https://doi.org/10.1016/0022-0248(95)00180-8)

- [33] M. D. Allendorf, T. H. Osterheld, C. F. Melius, The decomposition of methyltrichlorosilane in studies in a high-temperature flow reactor, *Mater. Res. Soc. Symp. Proc.* 334 (1-3) 105-110. <https://doi.org/10.1557/PROC-334-105>
- [34] H. S. Kim, D. J. Choi, Effect of diluent gases on growth behavior and characteristics of chemically vapor-deposited silicon carbide films, *J. Am. Ceram. Soc.* 82 (2) (1999) 331-337. <https://doi.org/10.1111/j.1551-2916.1999.tb20066.x>
- [35] G. Laduye, CVD du carbure de silicium à partir du système $\text{SiH}_x\text{Cl}_{4-x}/\text{C}_y\text{H}_z/\text{H}_2$ étude expérimentale et modélisation, PhD Thesis, University of Bordeaux, 2016. <https://tel.archives-ouvertes.fr/tel-01477657>
- [36] C. J. Mogab, H. J. Leamy, Conversion of Si to epitaxial SiC by reaction with C_2H_2 , *J. Appl. Phys.* 45 (1974) 1075-1084. <https://doi.org/10.1063/1.1663370>
- [37] G. M. Petrov, J. L. Giuliani, Model of a two-stage RF plasma reactor for SiC deposition, *J. App. Phys.* 90 (2001) 611-636. <https://doi.org/10.1063/1.1373701>
- [38] Ö. Danielsson, A. Henry, E. Janzén, Growth rate predictions of chemical vapor deposited silicon carbide epitaxial layers, *J. Cryst. Growth* 243 (2002) 170-184. [https://doi.org/10.1016/S0022-0248\(02\)01486-0](https://doi.org/10.1016/S0022-0248(02)01486-0)
- [39] P. Sukkaew, Ö. Danielsson, O. Kordina, E. Janzén, L. Ojamäe, Ab initio study of growth mechanism of 4H-SiC adsorption and surface reaction of C_2H_2 , C_2H_4 , CH_4 , and CH_3 , *J. Phys. Chem. C*. 121 (2017) 1241-1256. <https://doi.org/10.1021/acs.jpcc.6b11085>
- [40] E. López-Honorato, P. J. Meadows, J. Tan, P. Xiao, Control of stoichiometry, microstructure, and mechanical properties in SiC coatings produced by fluidized bed chemical vapor deposition, *J. Mater. Res.* 23 (2008) 1785-1796. <https://doi.org/10.1557/JMR.2008.0220>.
- [41] P. A. Tesner, Kinetics of pyrolytic carbon formation, in *Chemistry and Physics of Carbon*, Vol. 1, P. L. Walker Jr, P. A Throver eds., Marcel Dekker Inc., New York, 1984, pp. 65-161.
- [42] C. Pan, C. J. Chu, J. L. Margrave, R. H. Hauge, Chlorine-Activated Diamond Chemical Vapor Deposition, *J. Electrochem. Soc.* 141 (1994) 3246-3249. <http://dx.doi.org/10.1149/1.205312>

- [43] C. A. Rego, R. S. Tsang, P. W. May, M. N. R. Ashfold, K. N. Rosser, Gas phase composition measurements during chlorine assisted chemical vapor deposition of diamond: A molecular beam mass spectrometric study, *J. Appl. Phys.* 7 (1 6) 7264-7273. <https://doi.org/10.1063/1.361443>
- [44] G. D. Papasouliotis, S. V. Sotirchos, Steady State Multiplicity Phenomena in the Deposition of Silicon Carbide, *J. Electrochem. Soc.* 145 (1 8) 3 08-3 1 . <http://dx.doi.org/10.114 /1.18388 2>
- [45] I. M. Kostjulin, S. V. Sotirchos, Codeposition of SiC and C from Mixtures of Methyltrichlorosilane and Ethylene in Hydrogen, *Ind. Eng. Chem. Res.* 40 (2001) 2586-25 6. <https://doi.org/10.1021/ie000 60u>
- [46] I. M. Kostjulin, S. V. Sotirchos, Multiplicity of steady states in the codeposition of silicon carbide and carbon, *AIChE Journal* 48 (2002) 2 10-2 20. <https://doi.org/10.1002/aic.6 0481218>
- [47] C. Cavallotti, Reactivity of Silicon Surfaces in the Presence of Adsorbed Hydrogen and Chlorine, *Chem. Vap. Deposition* 16 (2010) 32 -335. <https://doi.org/10.1002/cvde.201006870>
- [48] A. Josiek, CVD dans le système $\text{CH}_3\text{SiCl}_3/\text{H}_2$: cinétiques expérimentales de dépôt de SiC et SiC+Si, modélisation, PhD Thesis, University of Bordeaux, 1 5. <http://www.theses.fr/1 5BOR10613>
- [4] R. Di Felice, C. A. Pignedoli, C. M. Bertoni, A. Catellani, P. L. Silvestrelli, C. Sbraccia, F. Ancilotto, M. Palumbo, O. Pulci, Ab initio investigation of the adsorption of organic molecules at Si(111) and Si(100) surfaces, *Surf. Sci.* 532-535 (2003) 82- 87. [https://dx.doi.org/10.1016/S003 -6028\(03\)00226-7](https://dx.doi.org/10.1016/S003 -6028(03)00226-7)
- [50] S. V. Sotirchos, G. D. Papasouliotis, Kinetic modeling of the deposition of SiC from methyltrichlorosilane, *MRS Proceedings*, Vol. 250 (Symposium R – Chemical Vapor Deposition of Refractory Metals and Ceramics II), T. M. Besman, B. M. Gallois, J. Warren eds., 1 1, pp. 35-40. <https://doi.org/10.1557/PROC-250-35>
- [51] F. Wang, D. S. Tsai, Low pressure chemical vapor deposition of silicon carbide from dichlorosilane and acetylene, *Mater. Chem. Phys.* 63 (2000) 1 6-201. [https://doi.org/10.1016/S0254-0584\(\)00207-2](https://doi.org/10.1016/S0254-0584()00207-2)

Figure captions

Figure 1 μ Multi-instrumented CVD reactor

Figure 2 μ (a) Arrhenius plot of the deposition rate R and (b) influence of the temperature T on the gas partial pressures P_i at the reactor outlet ($P = 2$ kPa, $\phi = 13$ and $Q_{tot} = 150$ sccm)

Figure 3 μ (a) Raman spectrum (from the outer surface) and (b) high resolution TEM image (inset μ selected area diffraction pattern) of a coating obtained at $T = 50$ °C, $P = 2$ kPa, $\phi = 13$ and $Q_{tot} = 150$ sccm

Figure 4 μ Raman spectra of coatings obtained at different temperatures T and at $P = 2$ kPa, $\phi = 13$ and $Q_{tot} = 150$ sccm (from polished cross sections)

Figure 5 μ Influence of the temperature T on the elemental composition of the solid deposit (measured upon heating, $\phi = 13$, $Q_{tot} = 150$ sccm)

Figure 6 μ TEM images of a coating obtained at $T = 1100$ °C, $P = 2$ kPa, $\phi = 13$ and $Q_{tot} = 150$ sccm. (a) bright field, (b) 111 dark field, (c) high resolution and (d) selected area diffraction pattern

Figure 7 μ Gas, solid and total mass yield of (a) Si and (b) C, (c) comparison of the total Si, C and Cl total mass yields ($P = 2$ kPa, $\phi = 13$ and $Q_{tot} = 150$ sccm)

Figure 8 μ (a) Arrhenius plot of the deposition rate R and (b) influence of the temperature T on the gas partial pressures P_i at the reactor outlet ($P = 5$ kPa, $\phi = 13$ and $Q_{tot} = 150$ sccm)

Figure 9 μ (a) Arrhenius plot of the deposition rate R and (b) influence of the temperature T on the gas partial pressures P_i at the reactor outlet ($P = 10$ kPa, $\phi = 13$ and $Q_{tot} = 150$ sccm)

Figure 10 μ Influence of the total gas flow rate Q_{tot} on the deposition rate R ($P = 2$ kPa, $\phi = 13$).

Figure 11 μ Influence of the gas residence time t_R on the partial pressures P_i at the reactor outlet ($P = 2$ kPa, $\phi = 13$, (a) $T = 50$ °C, (b) $T = 1100$ °C,

Figure 12 μ VTS decomposition kinetics, as deduced from the temperature dependence of the VTS partial pressure ($\phi = 13$, $Q_{tot} = 300$ sccm)

Figure 13 μ Influence of the total gas flow rate Q_{tot} on the deposition rate R , at different $P - T$ conditions ($\gamma = 13$, $Q_{tot} = 150$ sccm)

Figure 14 μ Influence of the VTS dilution ratio a on the deposition rate R ($P = 2$ kPa and $Q_{tot} = 150$ sccm)

Figure 15 μ Influence of the VTS dilution ratio a on the decomposition ratio of VTS ($P = 2$ kPa, $Q_{tot} = 150$ sccm)

Figure 16 μ Influence of the initial VTS partial pressure P_{VTS}^0 on (a) the deposition rate R and (b) the residual VTS partial pressure P_{VTS} at the reactor outlet ($P = 2-2.1$ kPa, $Q_{tot} = 205$ sccm).

Figure 17 μ Influence of the initial H_2 partial pressure $P_{H_2}^0$ on (a) the deposition rate R and (b) the residual VTS partial pressure P_{VTS} at the reactor outlet ($P = 2-2.5$ kPa, $Q_{tot} = 205$ sccm).

Figure 18 μ Influence of the VTS dilution in argon on (a) the deposition rate R and (b) the gas partial pressures P_i at the reactor outlet ($P_{Ar}^0/P_{VTS}^0 = 13$, $P = 2$ kPa, $Q_{tot} = 150$ sccm)

Figure 19 μ Influence of the (a) TCS (P_{TCS}^0), (b) C_2H_4 ($P_{C_2H_4}^0$) and (c) C_2H_2 ($P_{C_2H_2}^0$) partial pressure added in the initial gas phase on the deposition rate R ($P = 2-2.2$ kPa, $\gamma = 20$, $Q_{tot} = 205$ sccm).

Figure 20 μ Model porous substrates used for CVI experiments (a) before and (b) after assembling of the two graphite elements.

Figure 21 μ Normalized deposition rate along the various openings model channel pores ($x = 0$ at the entrance of the channel pore, $T = 1025$ °C, $P = 2$ kPa, $\gamma = 13$, $Q_{tot} = 300$ sccm)

Figure 22 μ Normalized deposition rate of pure SiC along the 300 mm-opening model channel pore ($x = 0$ at the entrance of the channel pore, $P = 2$ kPa, $\gamma = 13$, $Q_{tot} = 300$ sccm)

Figure 23 μ Comparison of the Arrhenius plots of the deposition rate at $P = 2$ kPa for MTS/ H_2 ($Q_{H_2}/Q_{MTS} = 10$, $Q_{tot} = 200$ sccm) [34], $SiHCl_3/C_2H_4/H_2$ ($Q_{H_2}/Q_{SiHCl_3} = 10$, $Q_{C_2H_4}/Q_{SiHCl_3} = 3/2$, $Q_{tot} = 250$ sccm) [34] and VTS/ H_2 ($\gamma = 12$, $Q_{tot} = 150$ sccm)

Figure 24 μ Comparison of the normalized deposition rate of pure SiC along the 300 mm-opening model channel pore, at $P = 2$ kPa, for MTS/ H_2 ($T = 70$ °C, $Q_{H_2}/Q_{MTS} = 3$, $Q_{tot} = 160$ sccm) [34],

SiHCl₃/C₃H₈/H₂ ($T = 70^\circ\text{C}$, $Q_{\text{H}_2}/Q_{\text{SiHCl}_3} = 10$, $Q_{\text{C}_3\text{H}_8}/Q_{\text{SiHCl}_3} = 1$, $Q_{\text{tot}} = 240$ sccm) [34] and VTS/H₂
($T = 50^\circ\text{C}$, $= 12$, $Q_{\text{tot}} = 150$ sccm)

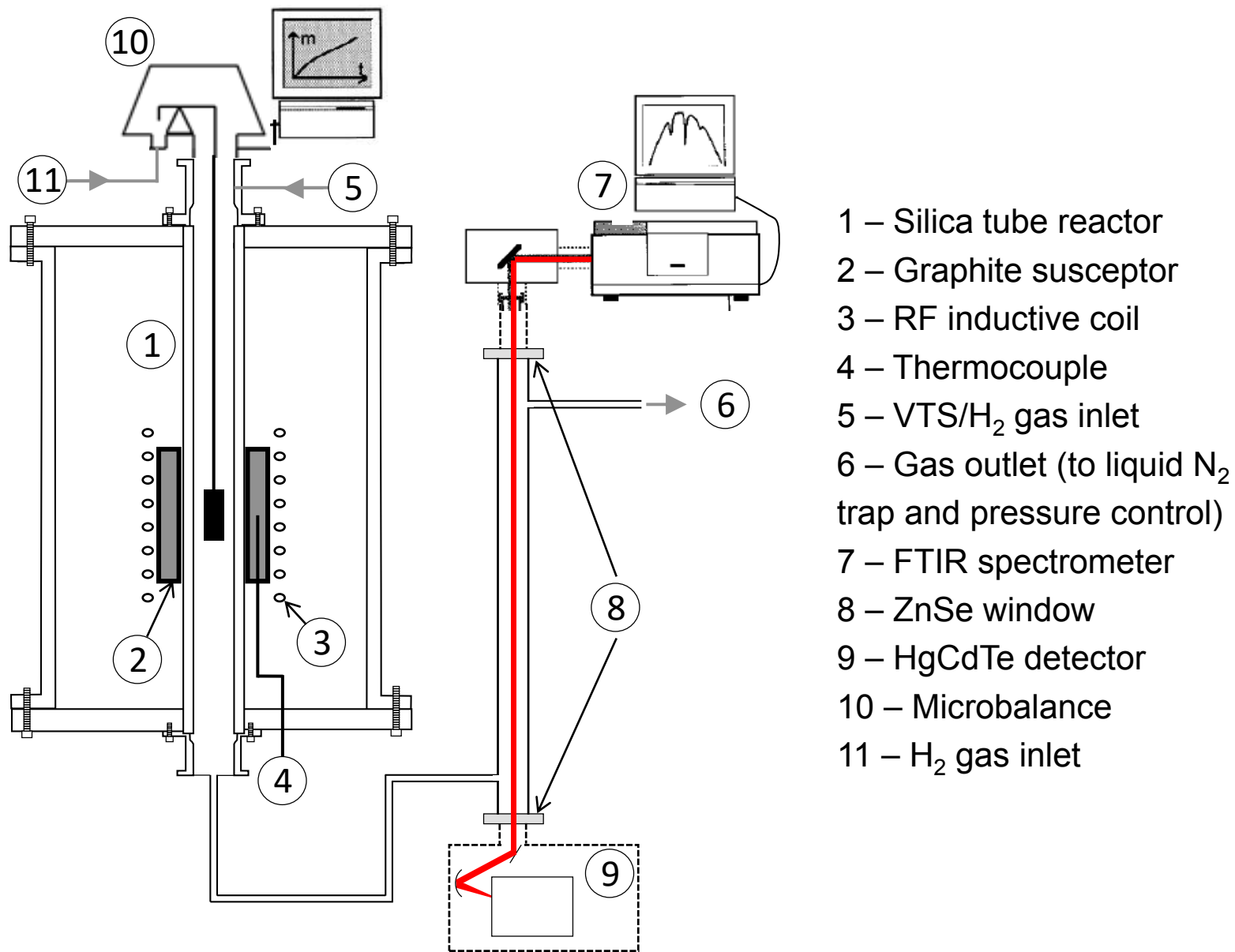


Figure 1: Multi-instrumented CVD reactor

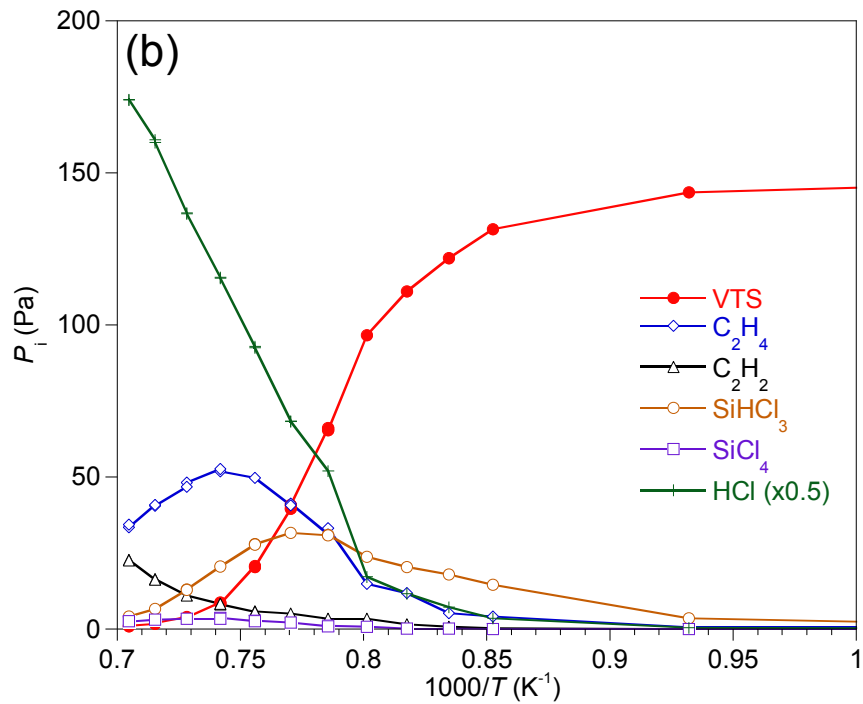
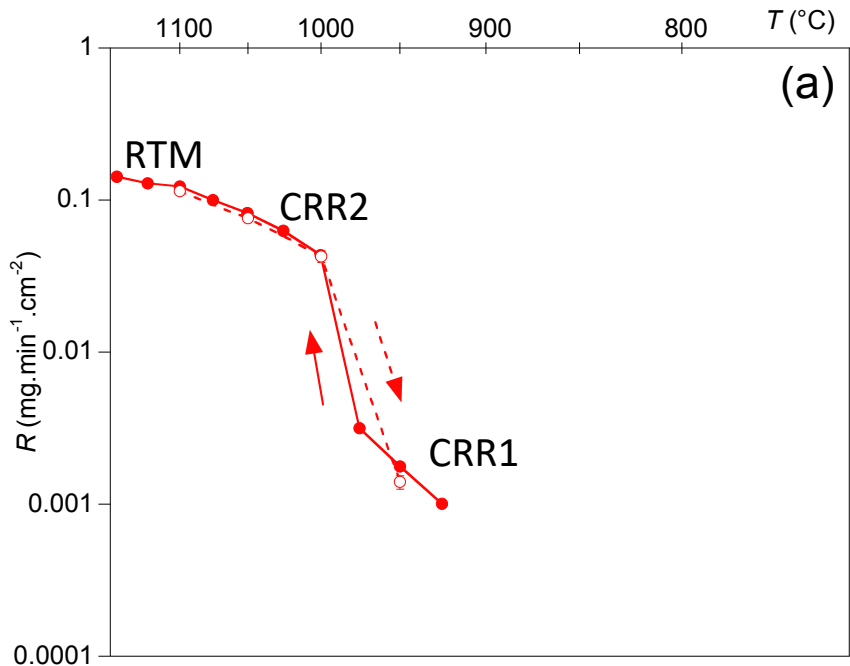


Figure 2: (a) Arrhenius plot of the deposition rate R and (b) influence of the temperature T on the gas partial pressures P_i at the reactor outlet ($P = 2$ kPa, $\tau = 13$ and $Q_{tot} = 150$ sccm)

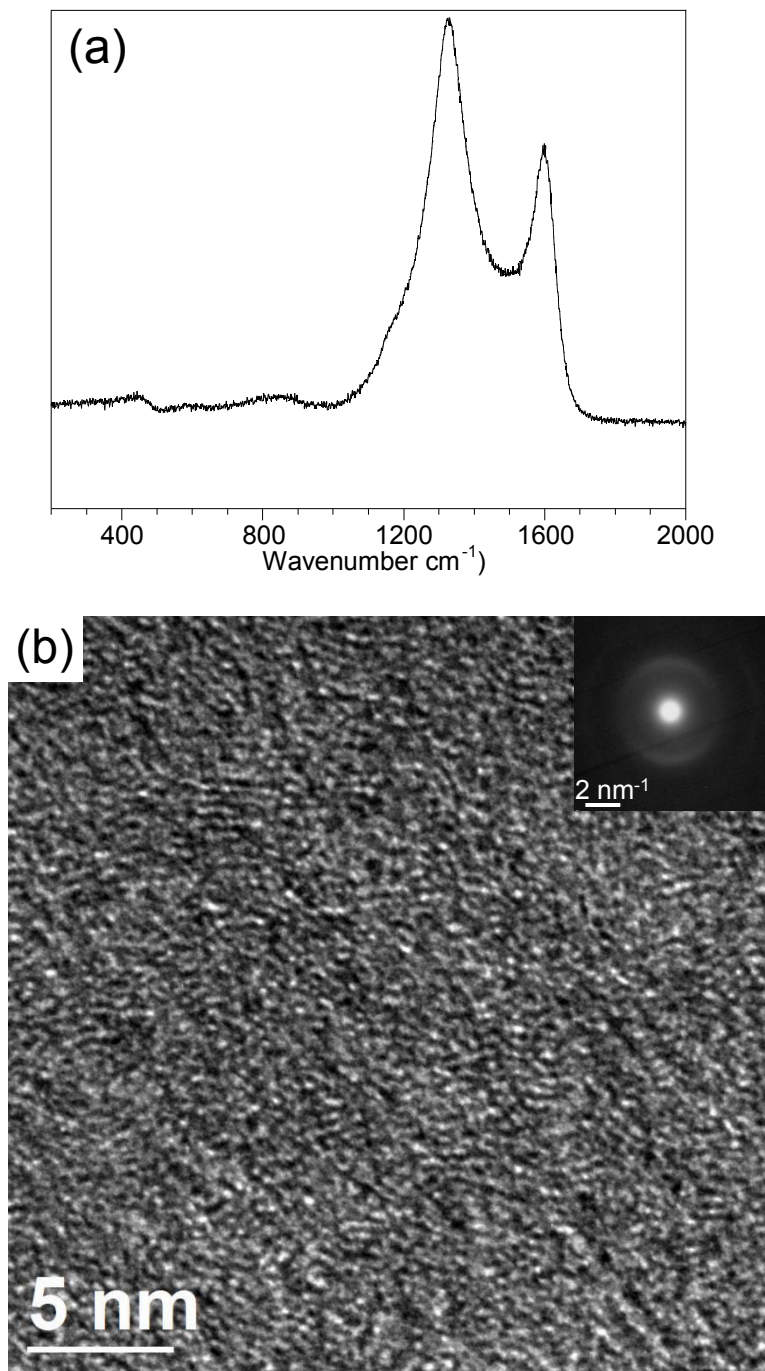


Figure 3: (a) Raman spectrum (from the outer surface) and (b) high resolution TEM image (inset: selected area diffraction pattern) of a coating obtained at $T = 950 \text{ }^\circ\text{C}$, $P = 2 \text{ kPa}$, $\dot{V} = 13$ and $Q_{tot} = 150 \text{ sccm}$

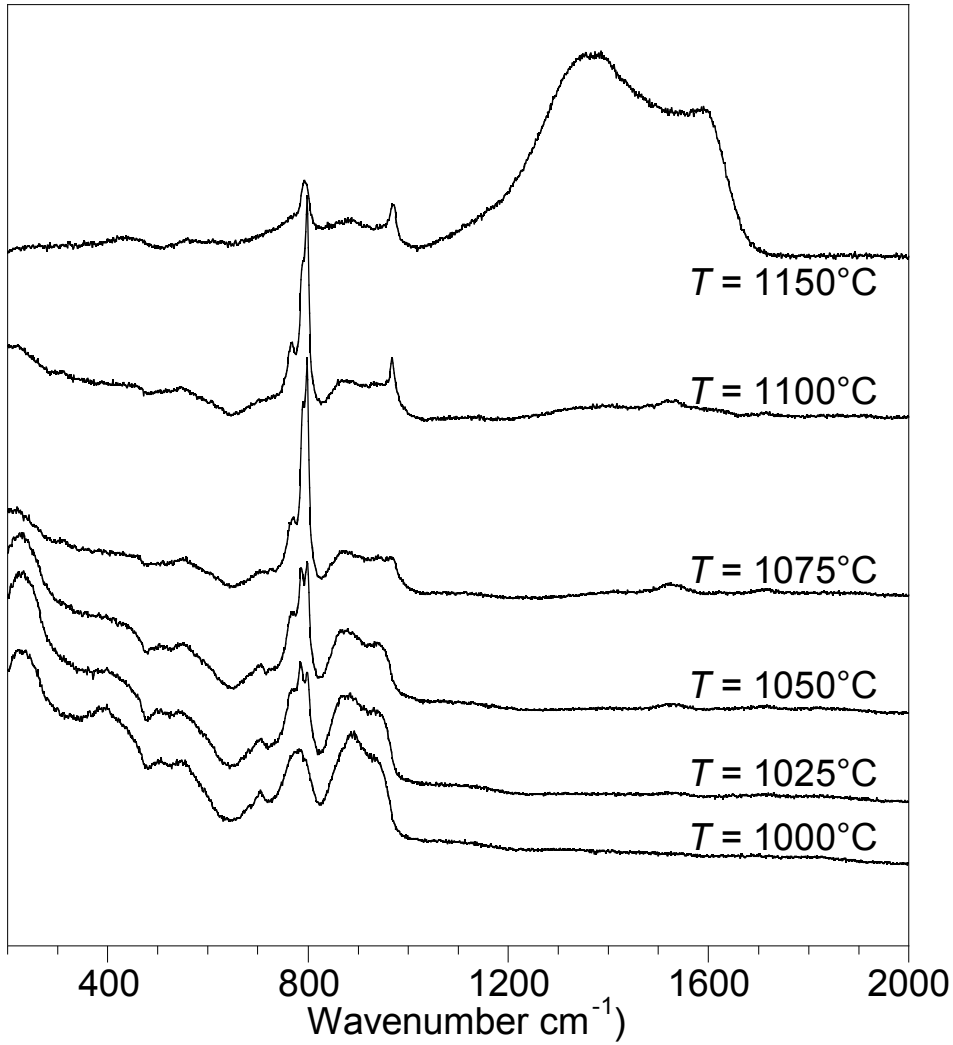


Figure 4: Raman spectra of coatings obtained at different temperatures T and at $P = 2$ kPa, $\phi = 13$ and $Q_{tot} = 150$ sccm (from polished cross sections)

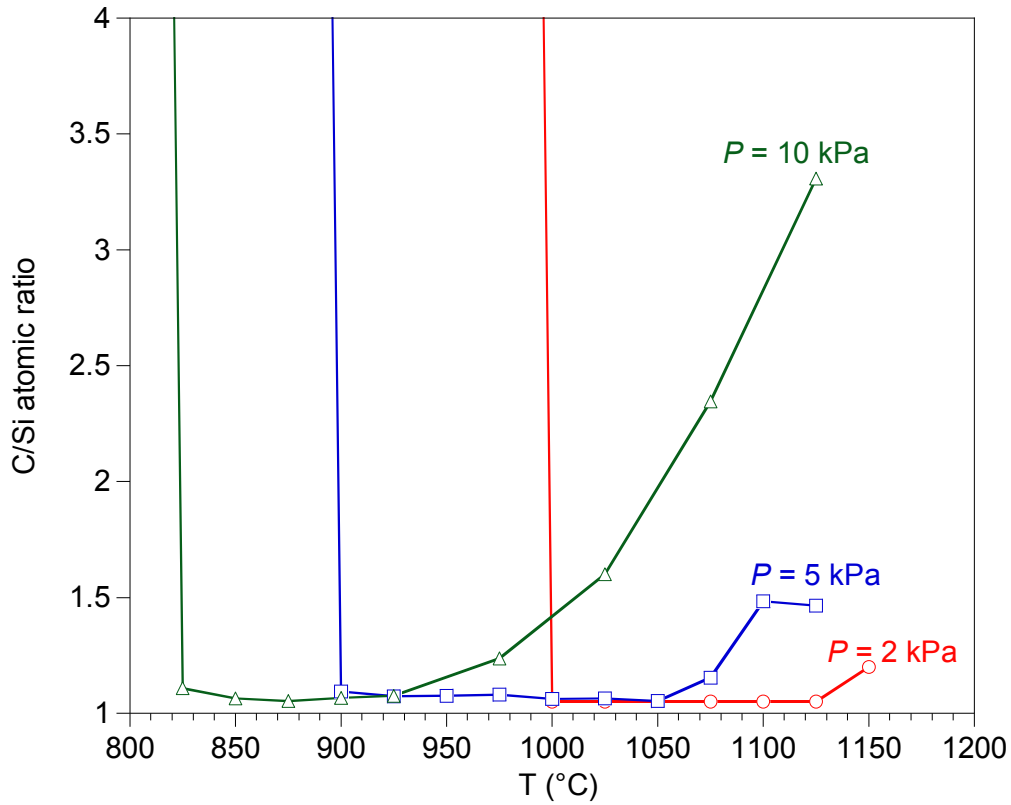


Figure 5: Influence of the temperature T on the elemental composition of the solid deposit (measured upon heating, $\dot{V} = 13$, $Q_{tot} = 150$ sccm)

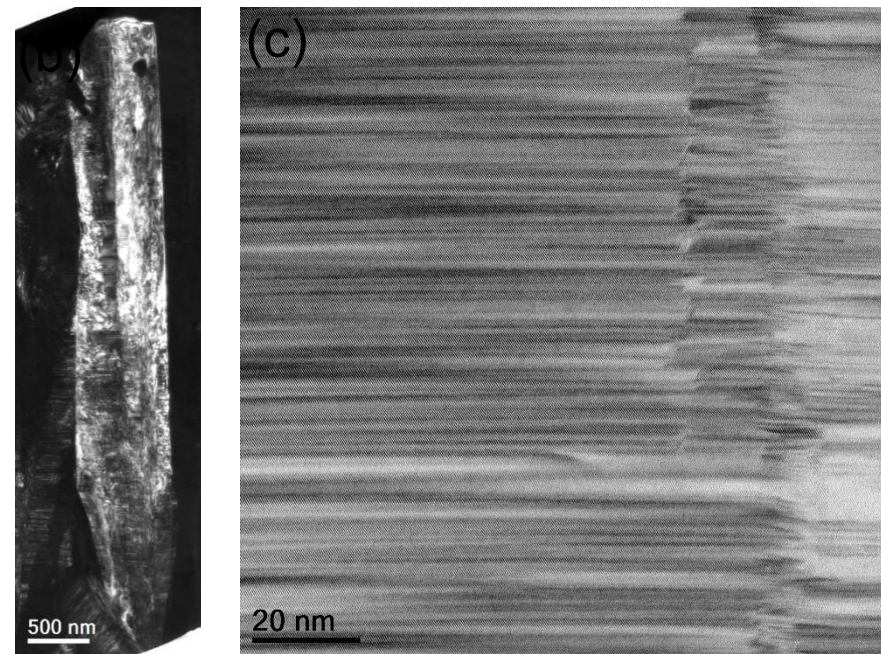
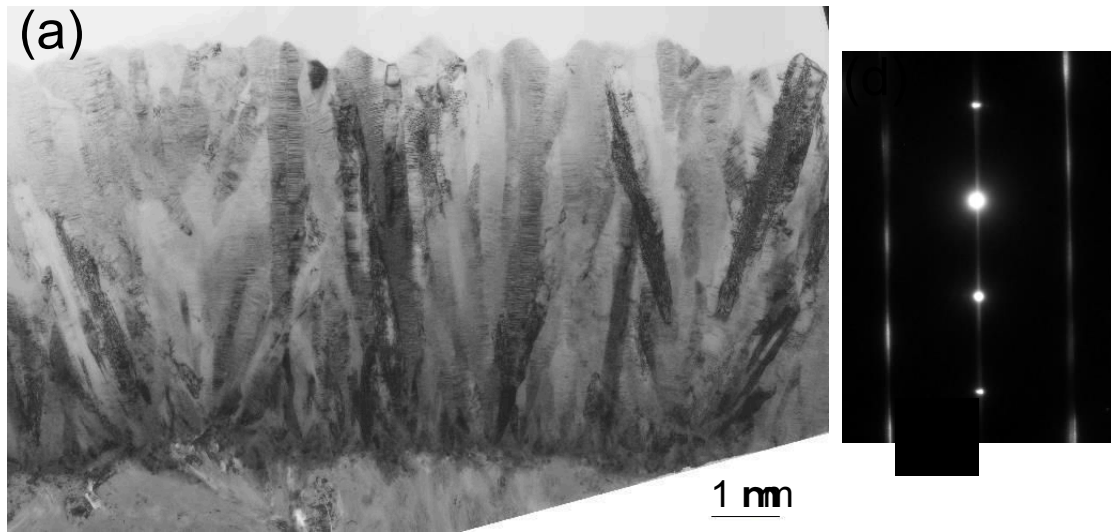


Figure 6: TEM images of a coating obtained at $T = 1100\text{ }^{\circ}\text{C}$, $P = 2\text{ kPa}$, $\dot{V} = 13$ and $Q_{tot} = 150$ sccm. (a) bright field, (b) 111 dark field, (c) high resolution and (d) selected area diffraction pattern

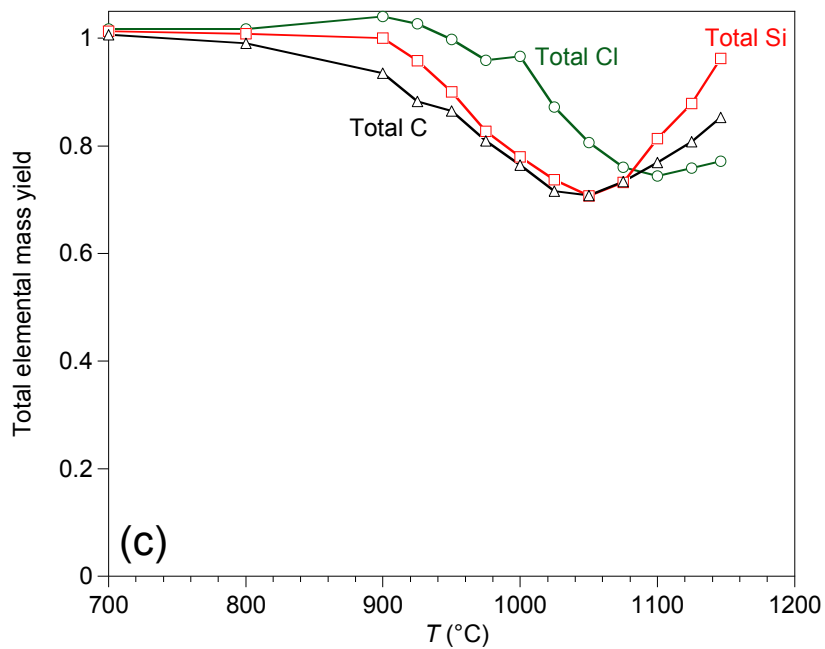
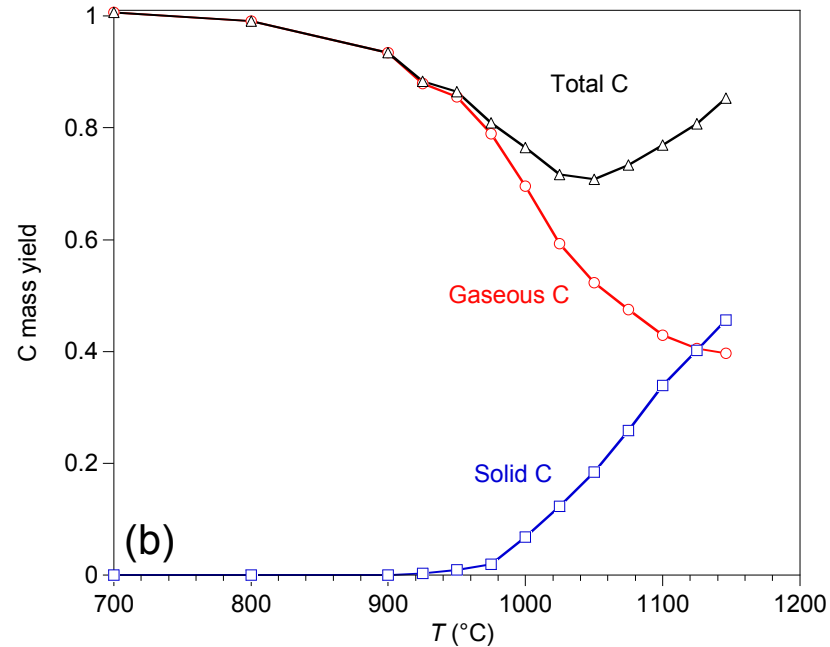
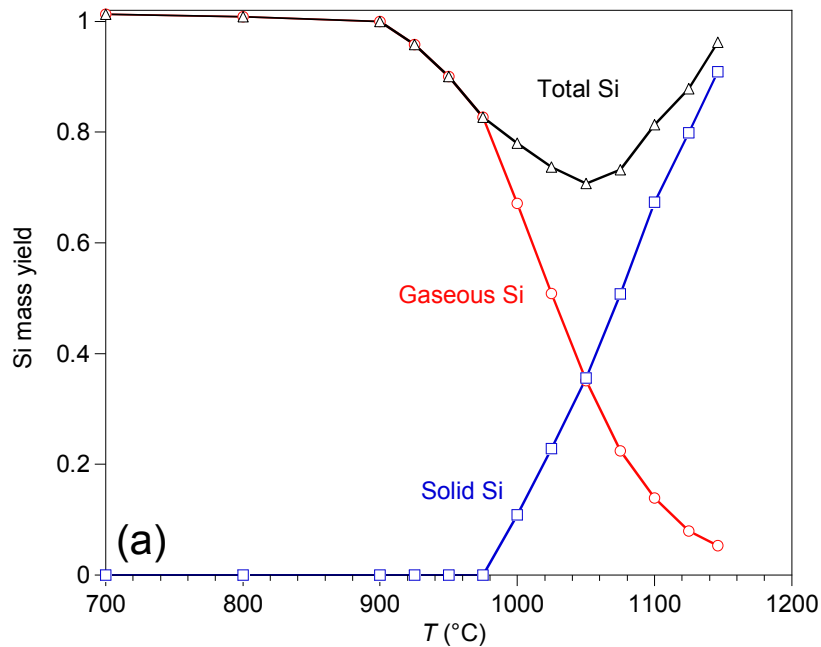


Figure 7: Gas, solid and total mass yield of (a) Si and (b) C, (c) comparison of the total Si, C and Cl total mass yields ($P = 2$ kPa, $\phi = 13$ and $Q_{tot} = 150$ sccm)

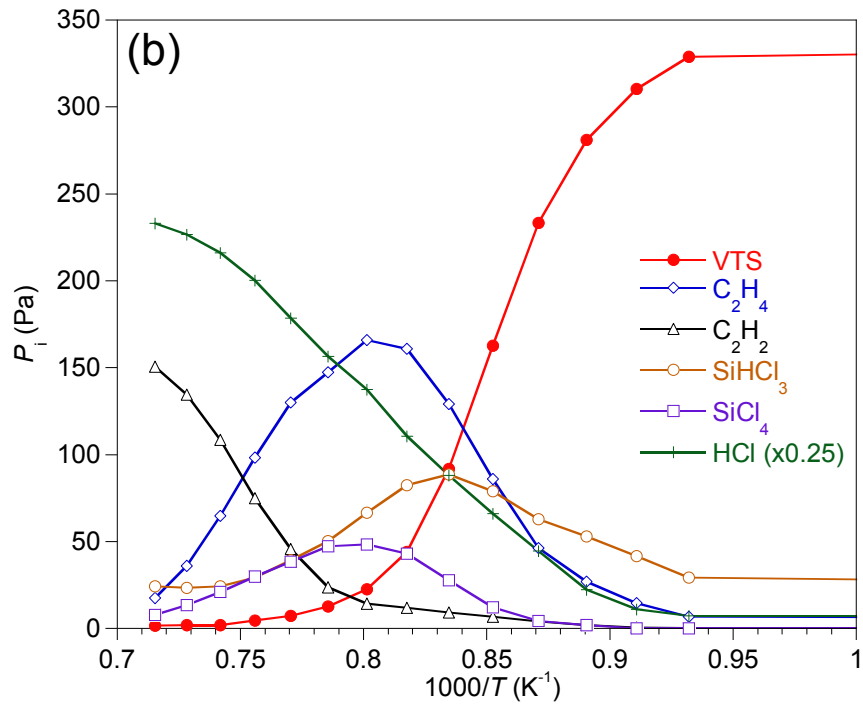
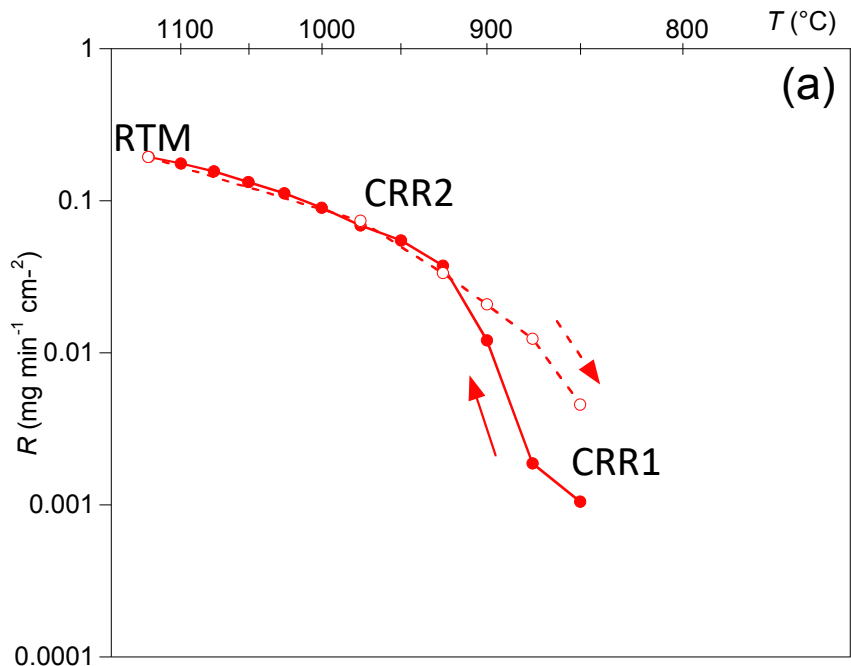


Figure 8: (a) Arrhenius plot of the deposition rate R and (b) influence of the temperature T on the gas partial pressures P_i at the reactor outlet ($P = 5$ kPa, $\tau = 13$ and $Q_{tot} = 150$ sccm)

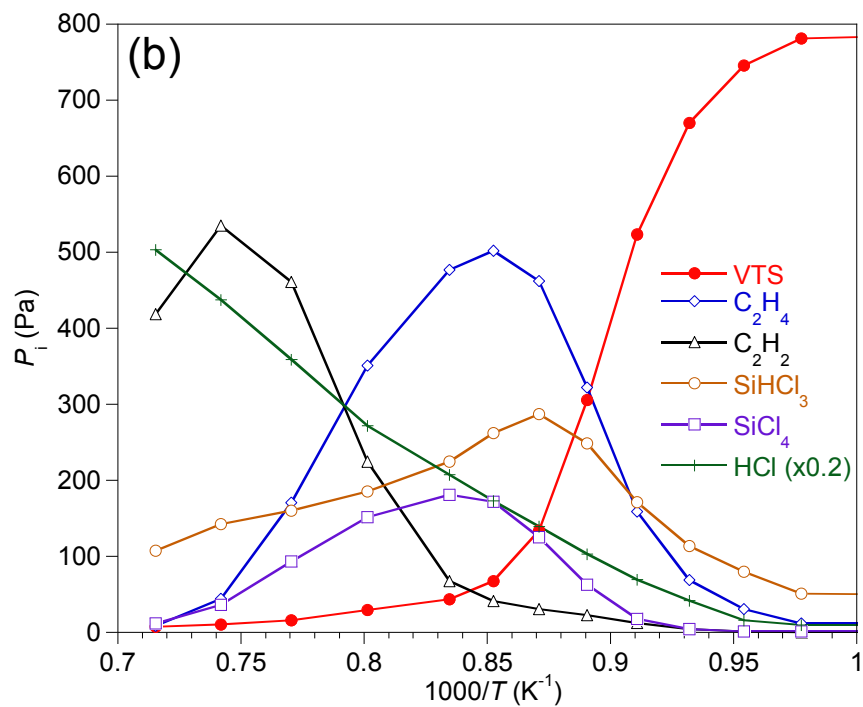
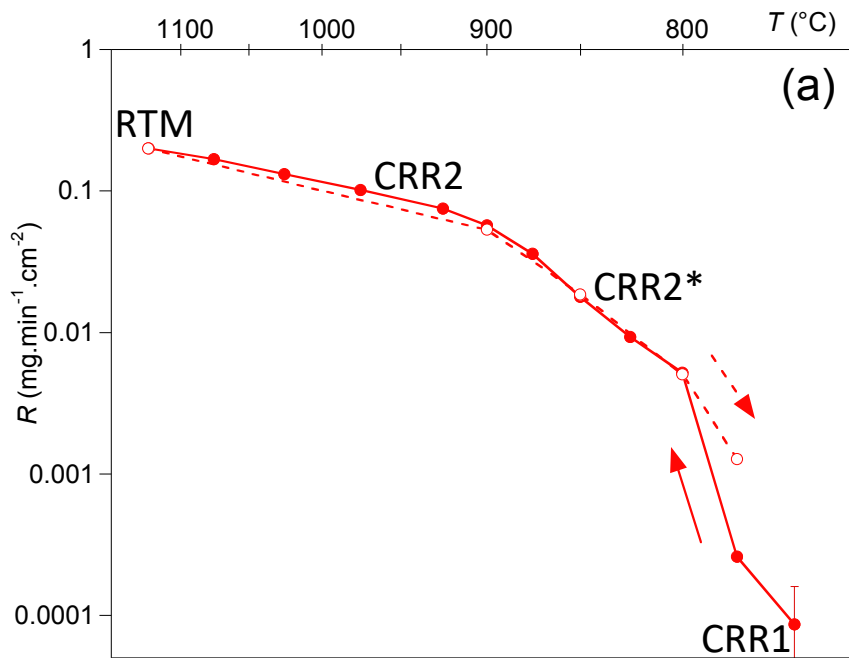


Figure 9: (a) Arrhenius plot of the deposition rate R and (b) influence of the temperature T on the gas partial pressures P_i at the reactor outlet ($P = 10$ kPa, $n = 13$ and $Q_{tot} = 150$ sccm)

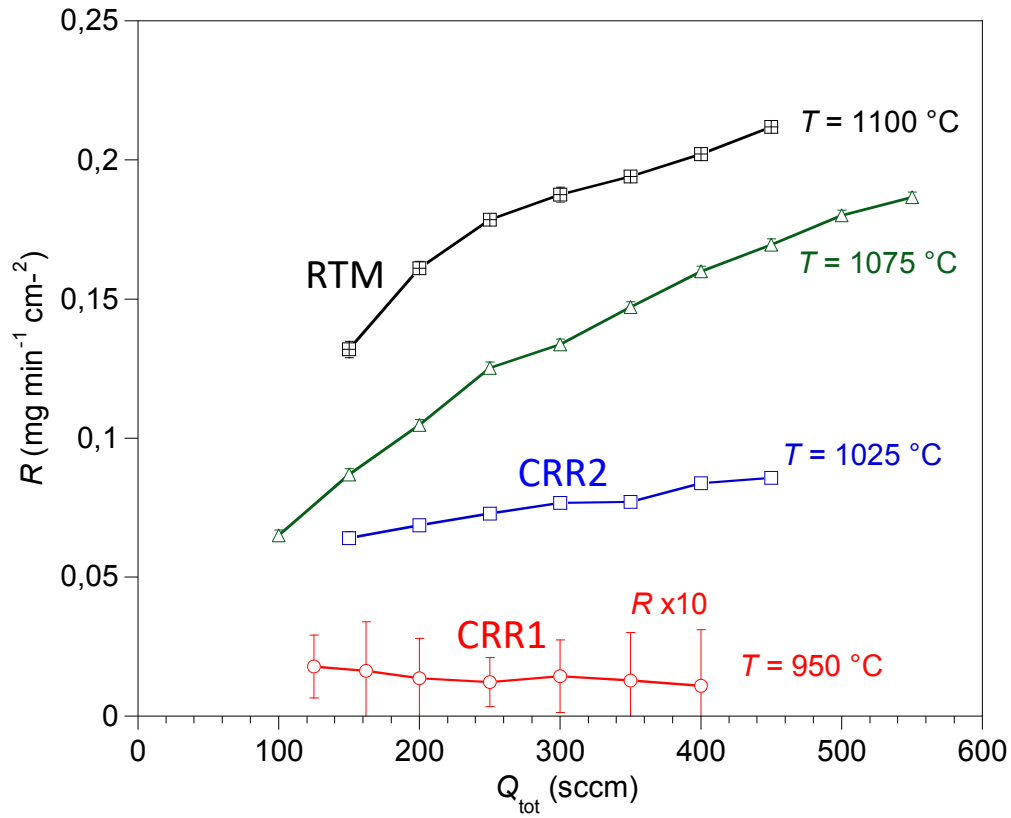


Figure 10: Influence of the total gas flow rate Q_{tot} on the deposition rate R ($P = 2 \text{ kPa}$, $\nu = 13$).

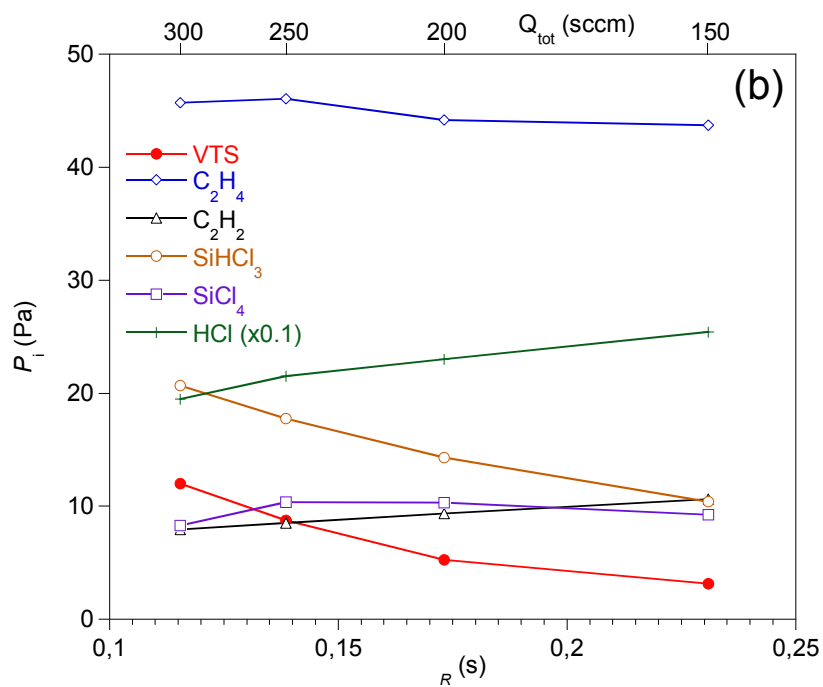
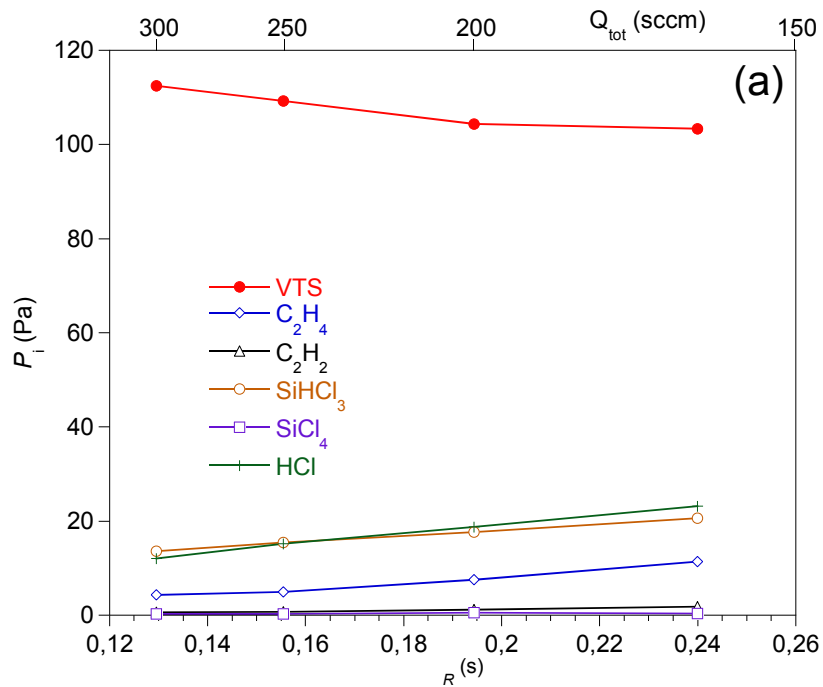


Figure 11: Influence of the gas residence time R on the partial pressures P_i at the reactor outlet ($P = 2 \text{ kPa}$, $\nu = 13$, (a) $T = 950^\circ\text{C}$, (b) $T = 1100^\circ\text{C}$,

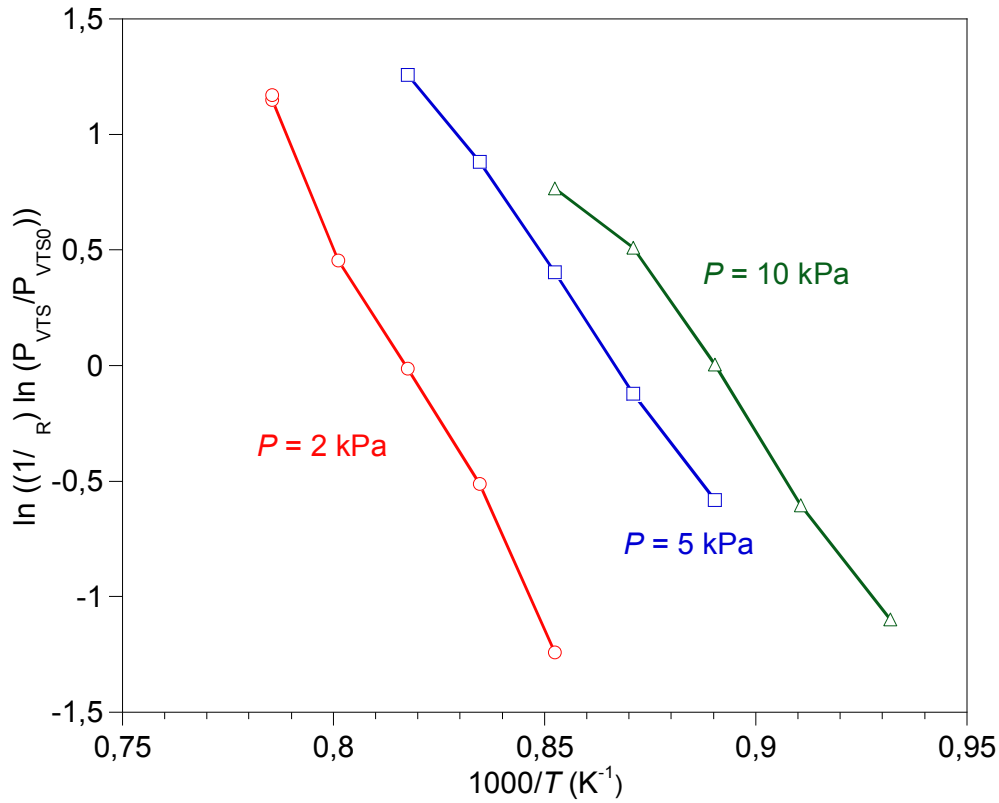


Figure 12: VTS decomposition kinetics, as deduced from the temperature dependence of the VTS partial pressure ($\nu = 13$, $Q_{tot} = 300$ sccm)

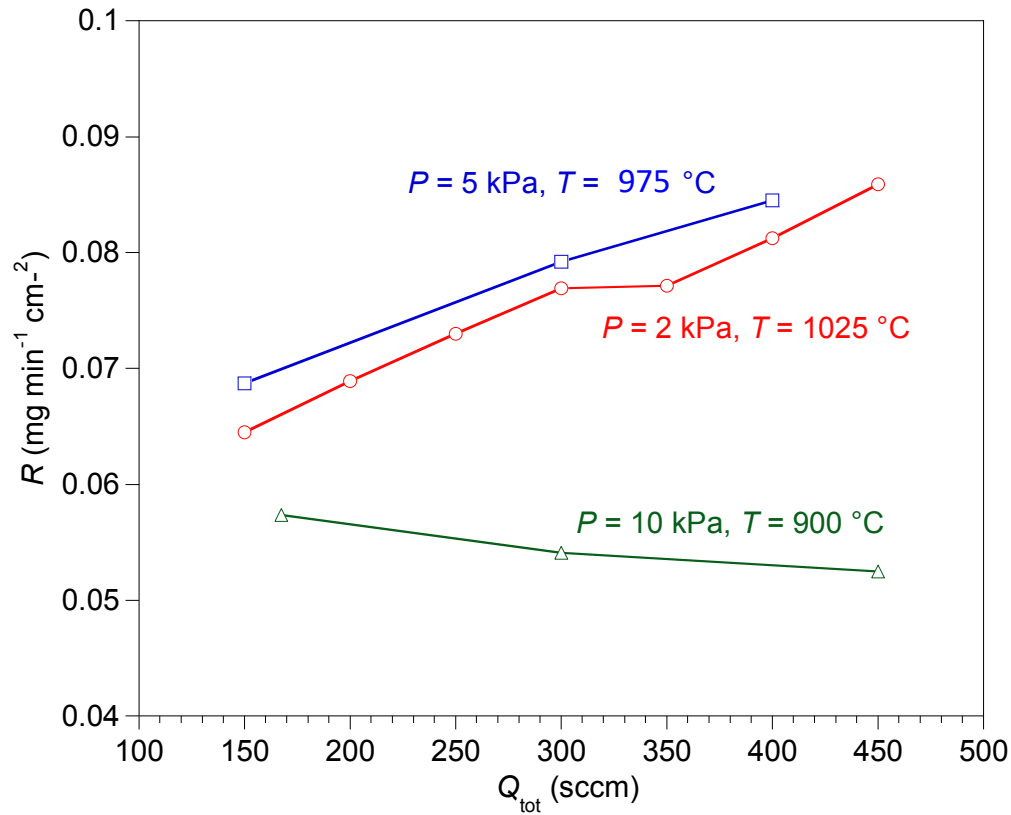


Figure 13: Influence of the total gas flow rate Q_{tot} on the deposition rate R , at different $P - T$ conditions ($Q_{tot} = 150$ sccm)

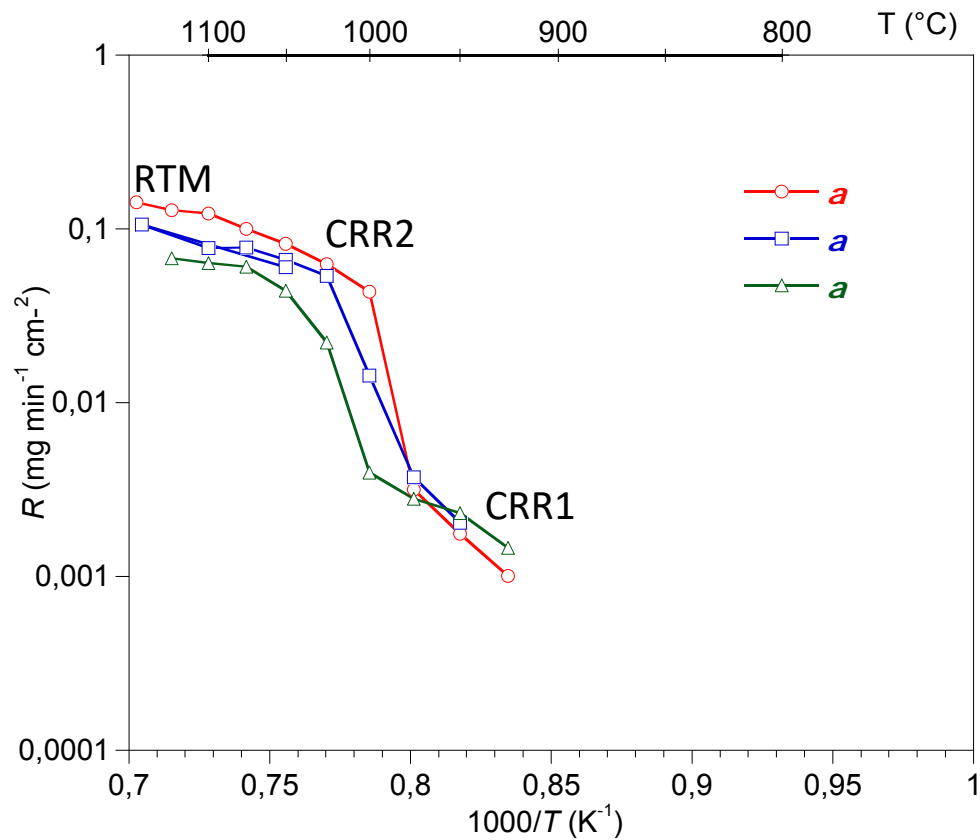


Figure 14: Influence of the VTS dilution ratio a on the deposition rate R ($P = 2 \text{ kPa}$ and $Q_{tot} = 150 \text{ sccm}$)

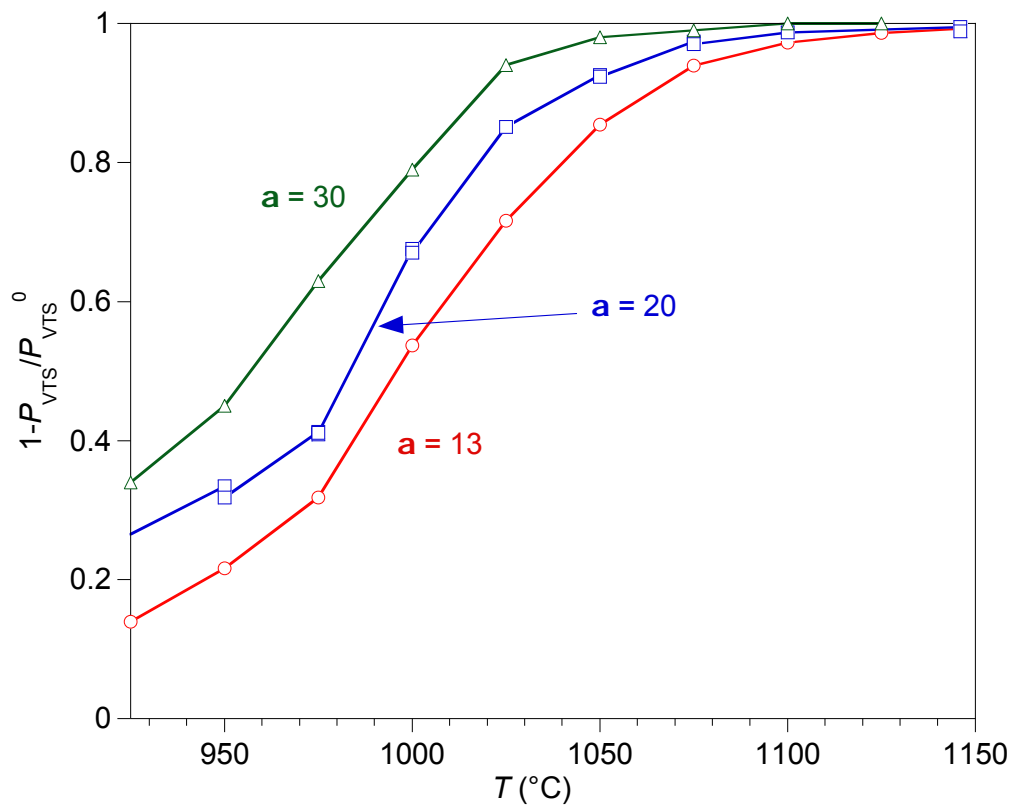


Figure 15: Influence of the VTS dilution ratio a on the decomposition ratio of VTS ($P = 2$ kPa, $Q_{tot} = 150$ sccm)

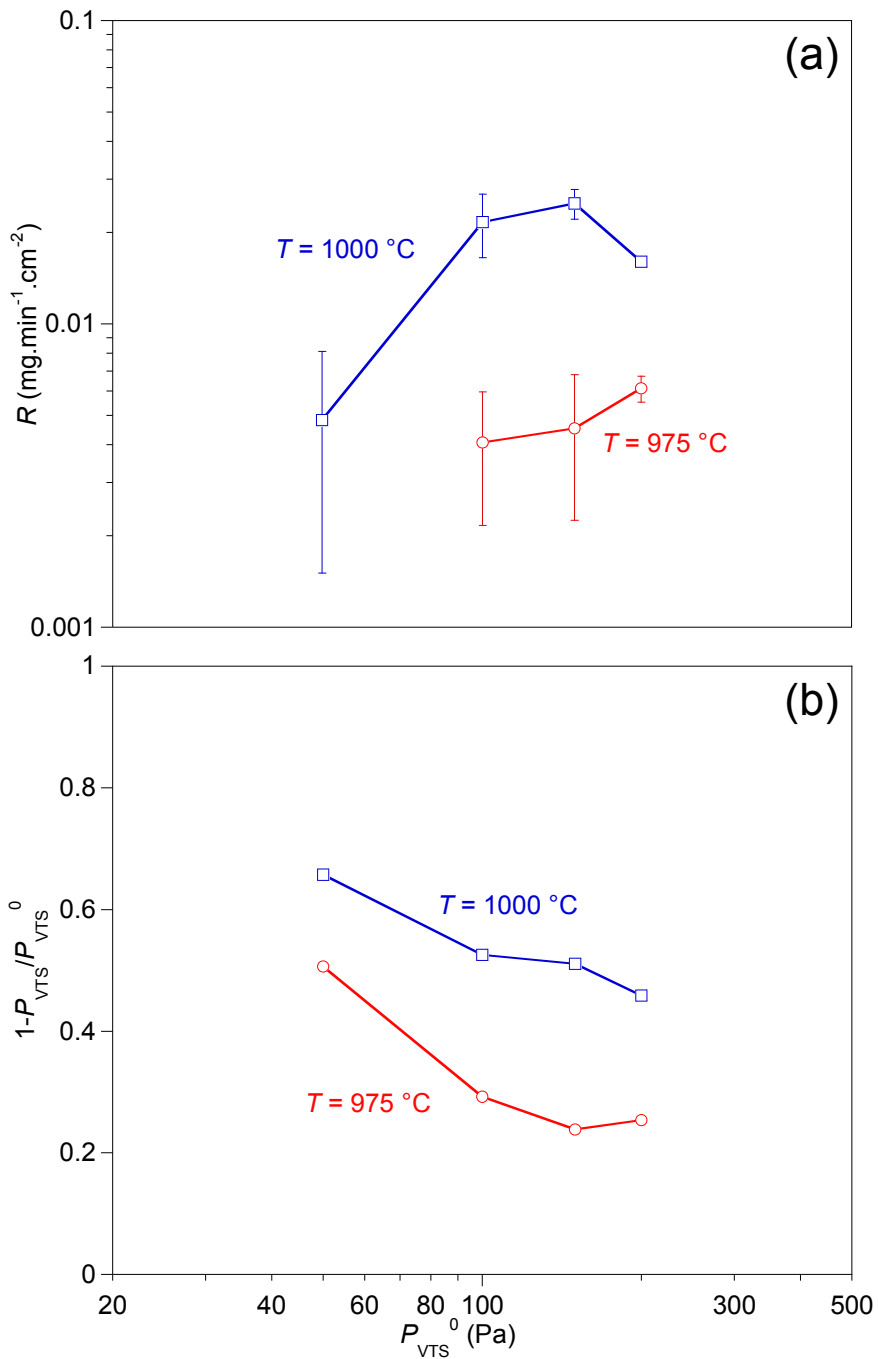


Figure 16: Influence of the initial VTS partial pressure P_{VTS}^0 on (a) the deposition rate R and (b) the residual VTS partial pressure P_{VTS} at the reactor outlet ($P = 2\text{-}2.1 \text{ kPa}$, $Q_{\text{tot}} = 205 \text{ sccm}$).

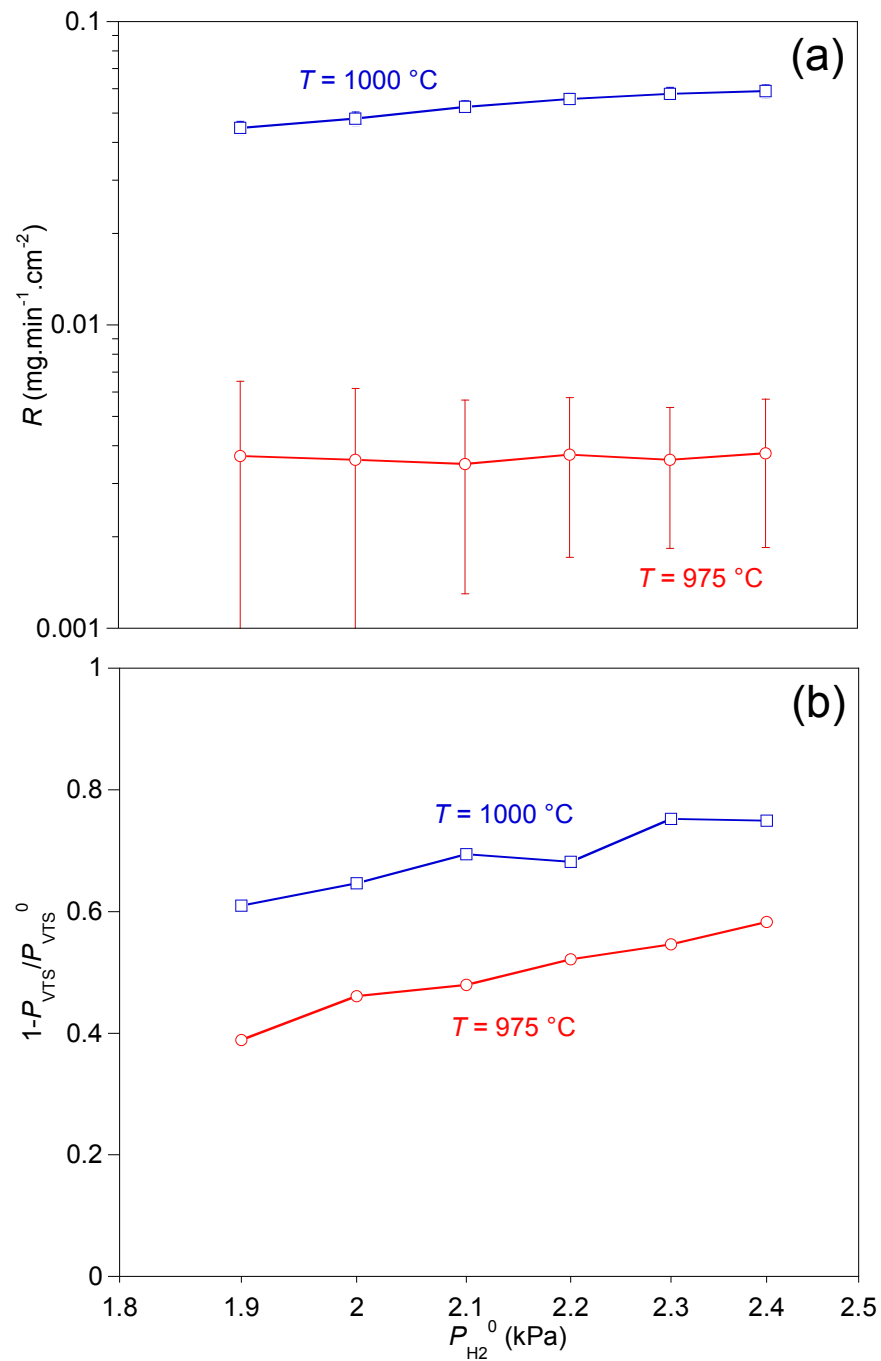


Figure 17: Influence of the initial H_2 partial pressure $P_{H_2}^0$ on (a) the deposition rate R and (b) the residual VTS partial pressure P_{VTS} at the reactor outlet ($P = 2\text{-}2.5\text{ kPa}$, $Q_{\text{tot}} = 205\text{ sccm}$).

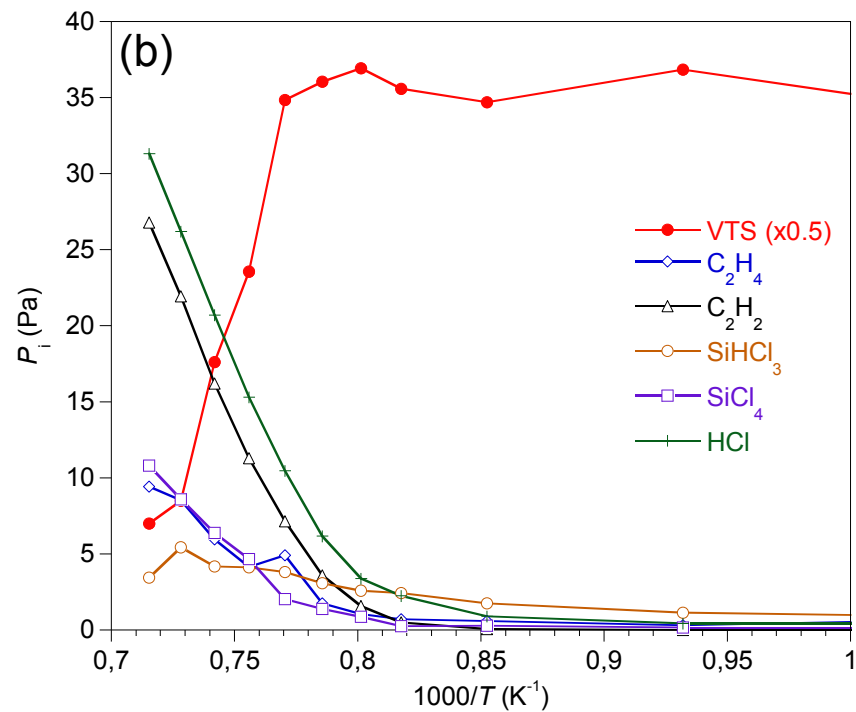
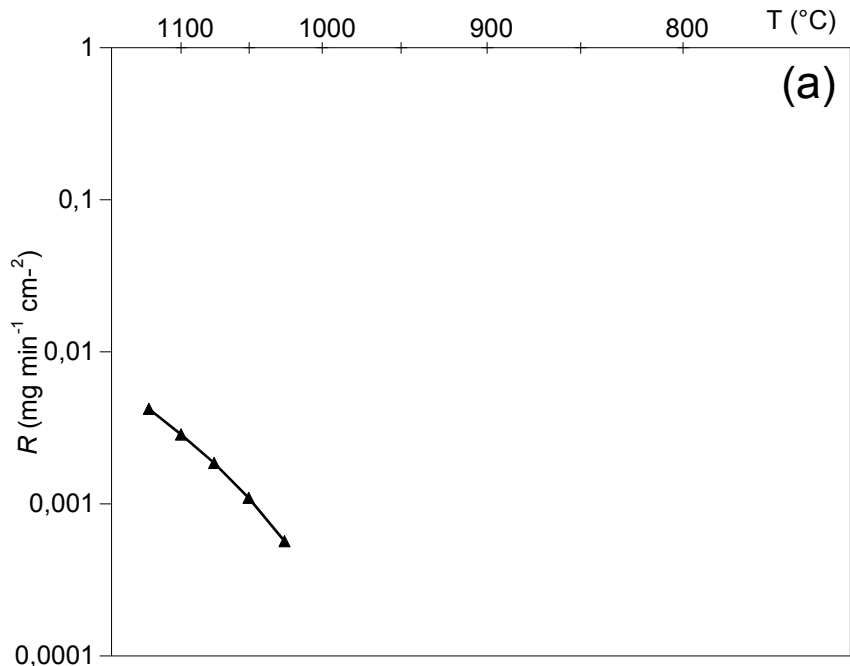


Figure 18: Influence of the VTS dilution in argon on (a) the deposition rate R and (b) the gas partial pressures P_i at the reactor outlet ($P_{\text{Ar}}^0/P_{\text{VTS}}^0 = 13$, $P = 2$ kPa, $Q_{\text{tot}} = 150$ sccm)

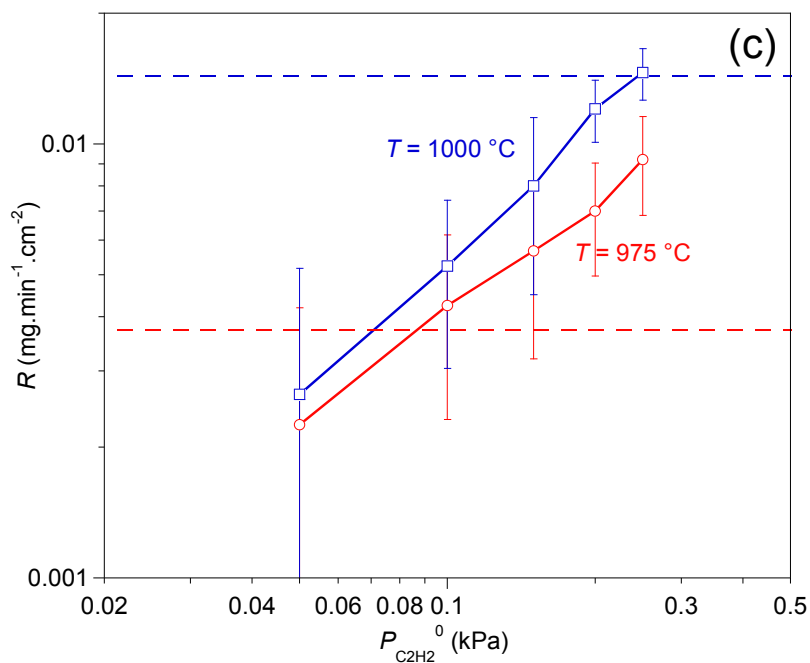
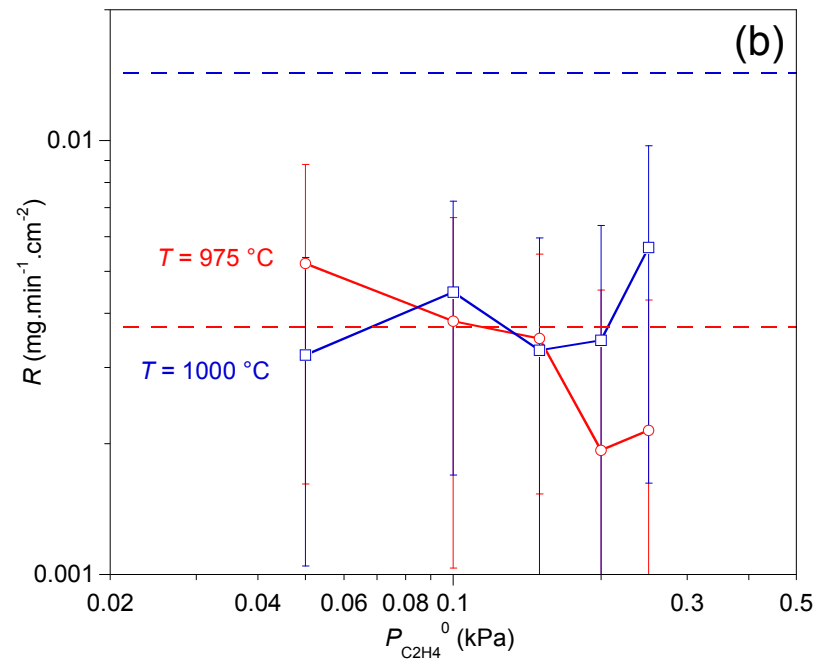
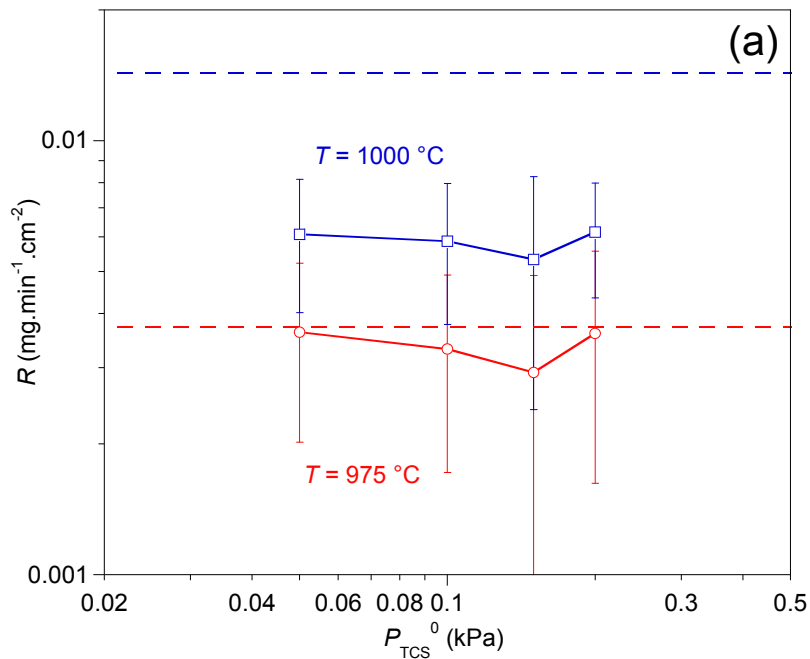


Figure 19: Influence of the (a) TCS (P_{TCS}^0), (b) C₂H₄ ($P_{C_2H_4}^0$) and (c) C₂H₂ ($P_{C_2H_2}^0$) partial pressure added in the initial gas phase on the deposition rate R ($P = 2\text{-}2.2\text{ kPa}$, $\tau = 20$, $Q_{tot} = 205\text{ sccm}$). Horizontal dotted lines indicate the R values obtained without gas product addition.

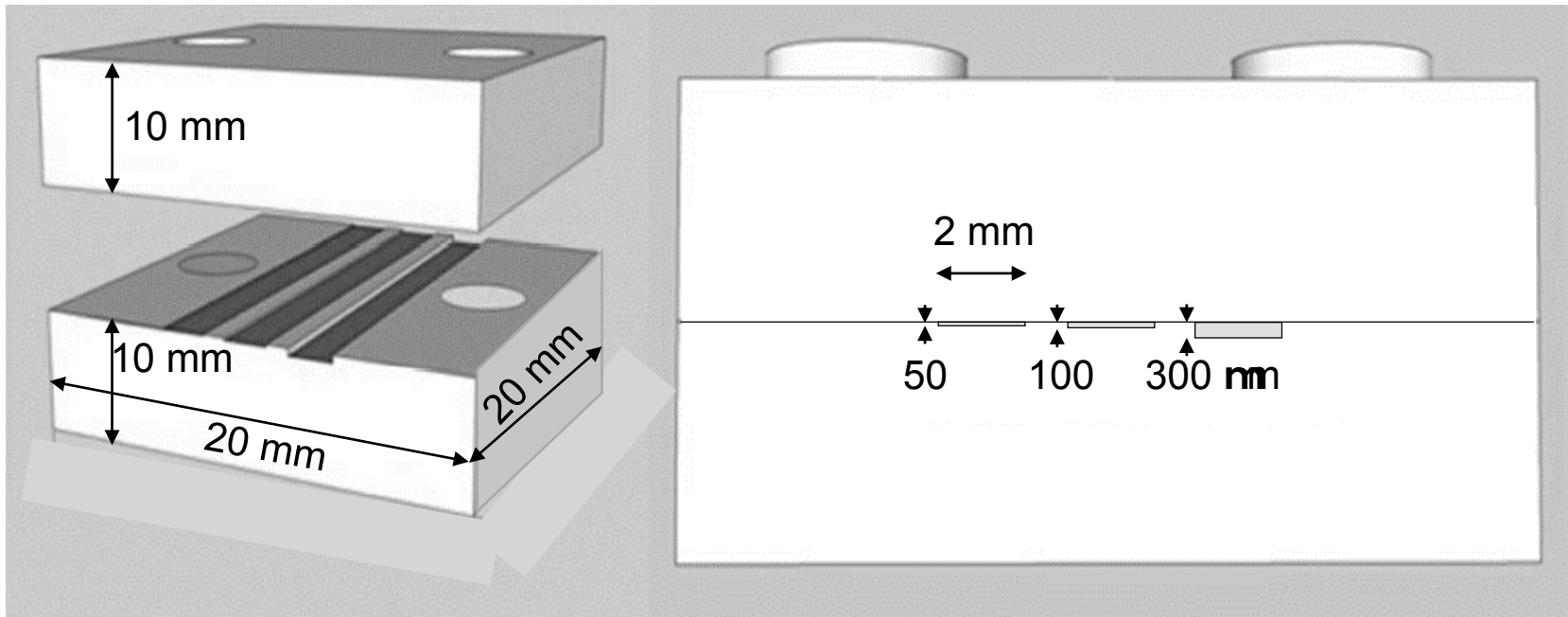


Figure 20: Model porous substrates used for CVD experiments (a) before *and* (b) after assembling of the two graphite elements.

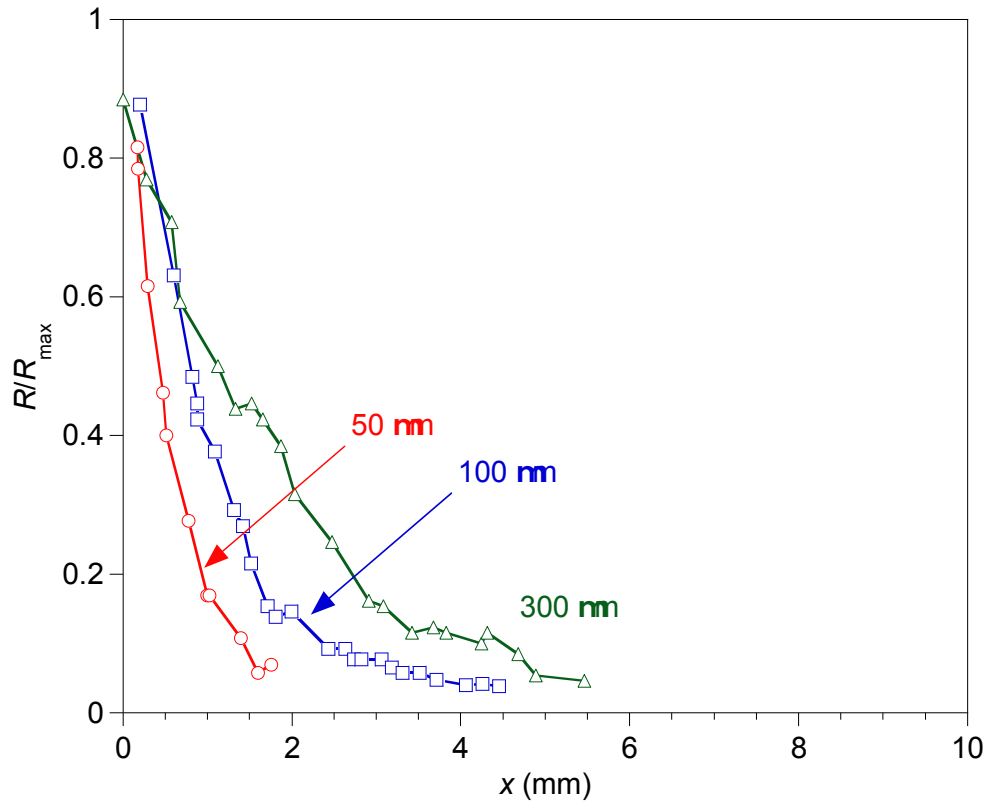


Figure 21: Normalized deposition rate along the various openings model channel pores ($x = 0$ at the entrance of the channel pore, $T = 1025$ °C, $P = 2$ kPa, $\nu = 13$, $Q_{tot} = 300$ sccm)

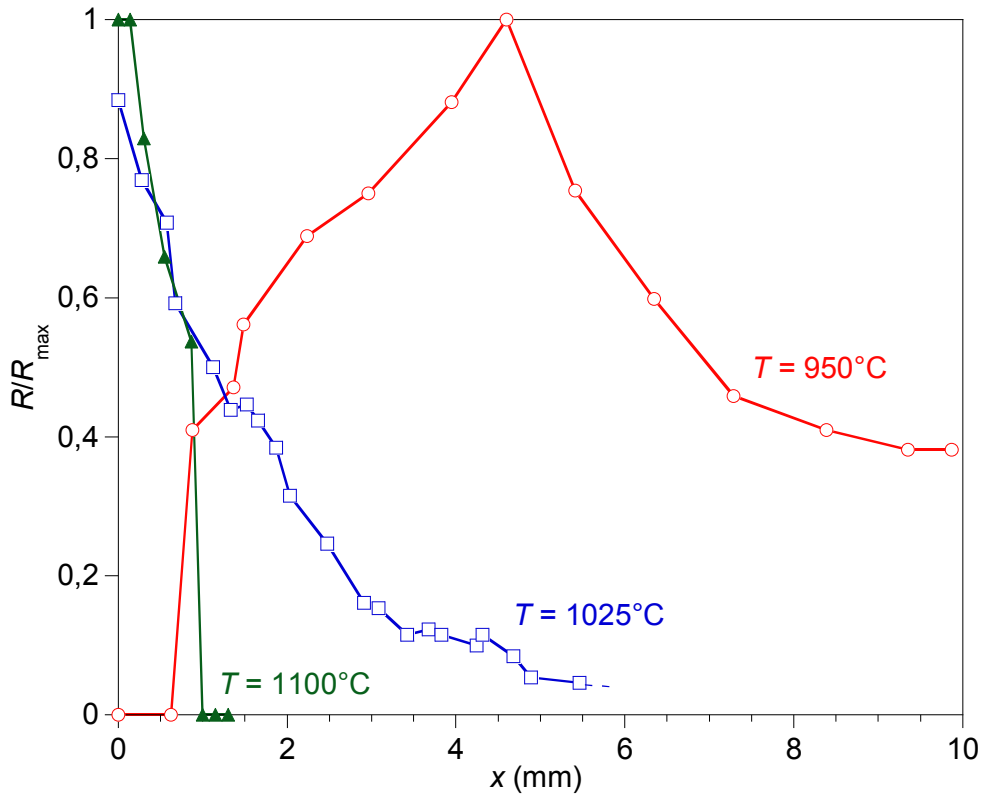


Figure 22: Normalized deposition rate of pure SiC along the 300 μm -opening model channel pore ($x = 0$ at the entrance of the channel pore, $P = 2$ kPa, $\text{Re} = 13$, $Q_{\text{tot}} = 300$ sccm)

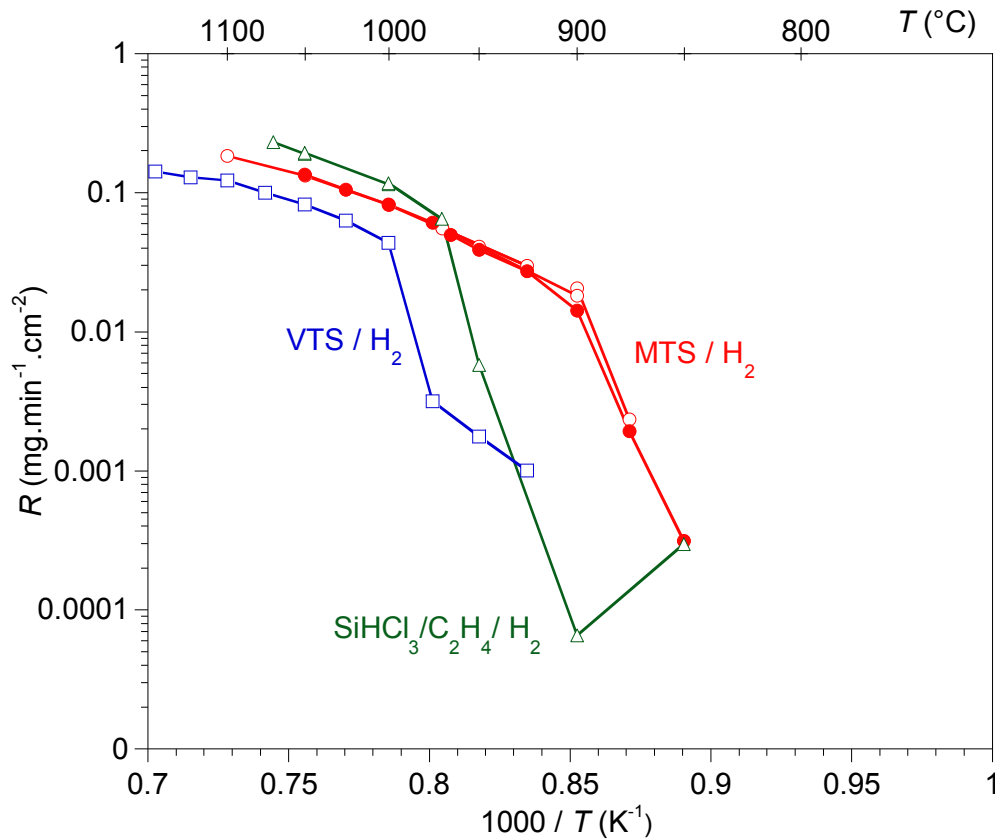


Figure 23: Comparison of the Arrhenius plots of the deposition rate at $P = 2$ kPa for MTS/H₂ ($Q_{\text{H}_2}/Q_{\text{MTS}} = 10$, $Q_{\text{tot}} = 200$ sccm) [34], SiHCl₃/C₂H₄/H₂ ($Q_{\text{H}_2}/Q_{\text{SiHCl}_3} = 10$, $Q_{\text{C}_2\text{H}_4}/Q_{\text{SiHCl}_3} = 3/2$, $Q_{\text{tot}} = 250$ sccm) [34] and VTS/H₂ ($Q_{\text{H}_2}/Q_{\text{VTS}} = 13$, $Q_{\text{tot}} = 150$ sccm)

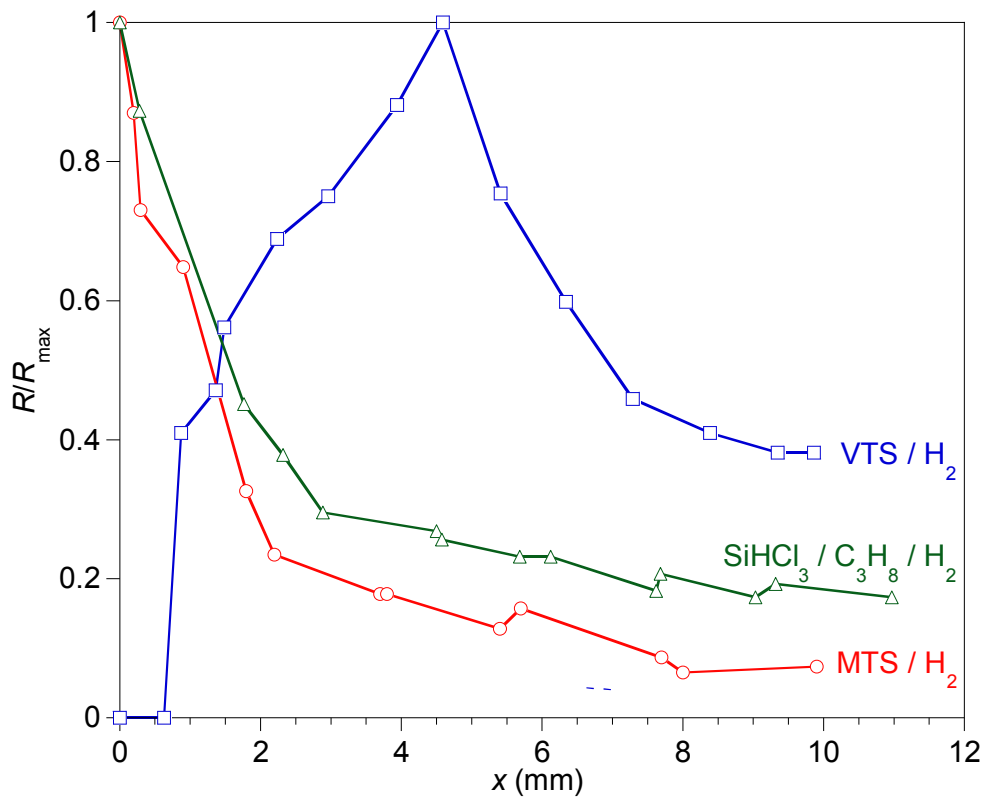


Figure 24: Comparison of the normalized deposition rate of pure SiC along the 300 μm -opening model channel pore, at $P = 2$ kPa, for MTS/H₂ ($T = 970^\circ\text{C}$, $Q_{\text{H}_2}/Q_{\text{MTS}} = 3$, $Q_{\text{tot}} = 160$ sccm) [34], SiHCl₃/C₃H₈/H₂ ($T = 970^\circ\text{C}$, $Q_{\text{H}_2}/Q_{\text{SiHCl}_3} = 10$, $Q_{\text{C}_3\text{H}_8}/Q_{\text{SiHCl}_3} = 1$, $Q_{\text{tot}} = 240$ sccm) [34] and VTS/H₂ ($T = 950^\circ\text{C}$, $Q_{\text{H}_2}/Q_{\text{VTS}} = 12$, $Q_{\text{tot}} = 150$ sccm)

Supplementary material 1/3

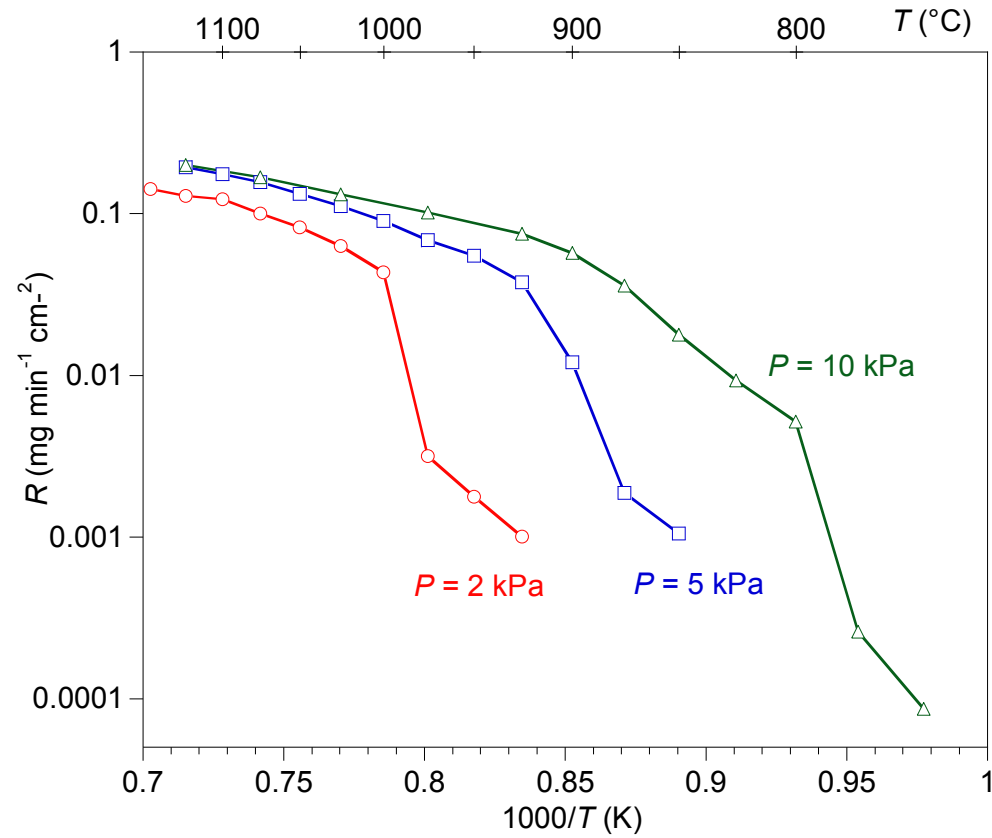


Figure SI1: Arrhenius plots of the deposition rate R at different pressures ($v = 13$ and $Q_{tot} = 150$ sccm)

Supplementary material 2/3

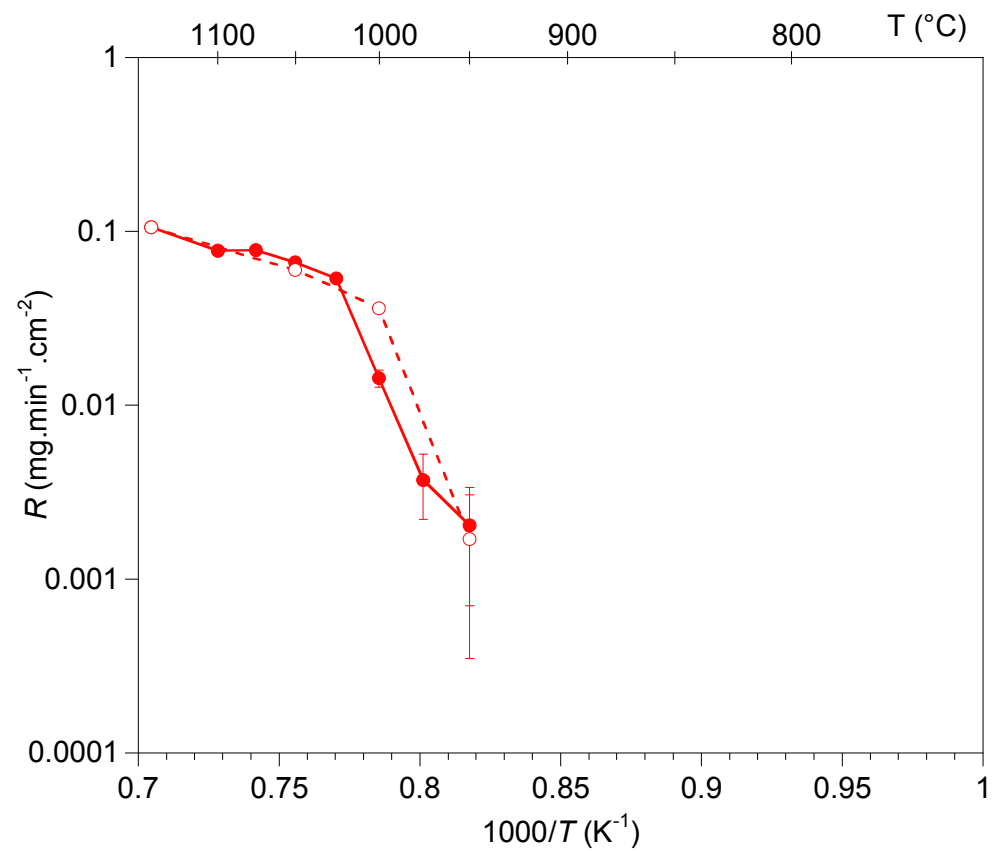


Figure SI2: Arrhenius plot of the deposition rate R ($P = 2$ kPa, $\nu = 20$ and $Q_{tot} = 150$ sccm)

Supplementary material 3/3

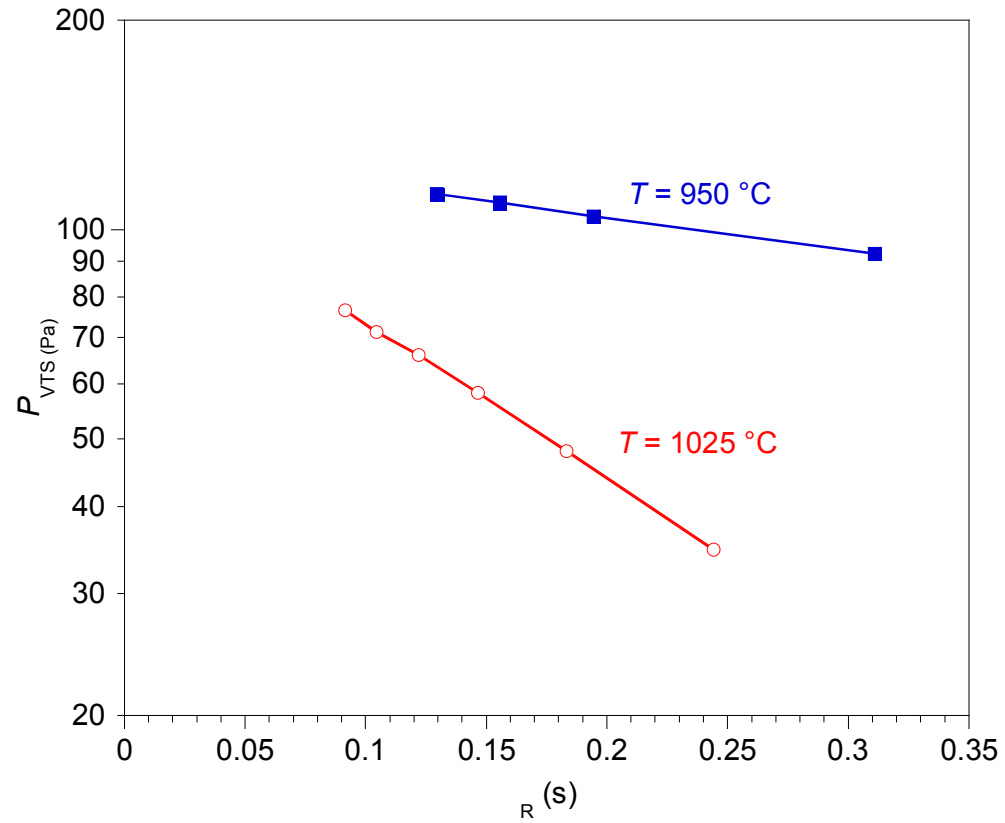


Figure SI3: Kinetics of VTS homogeneous decomposition ($P = 2$ kPa, $n = 12$)